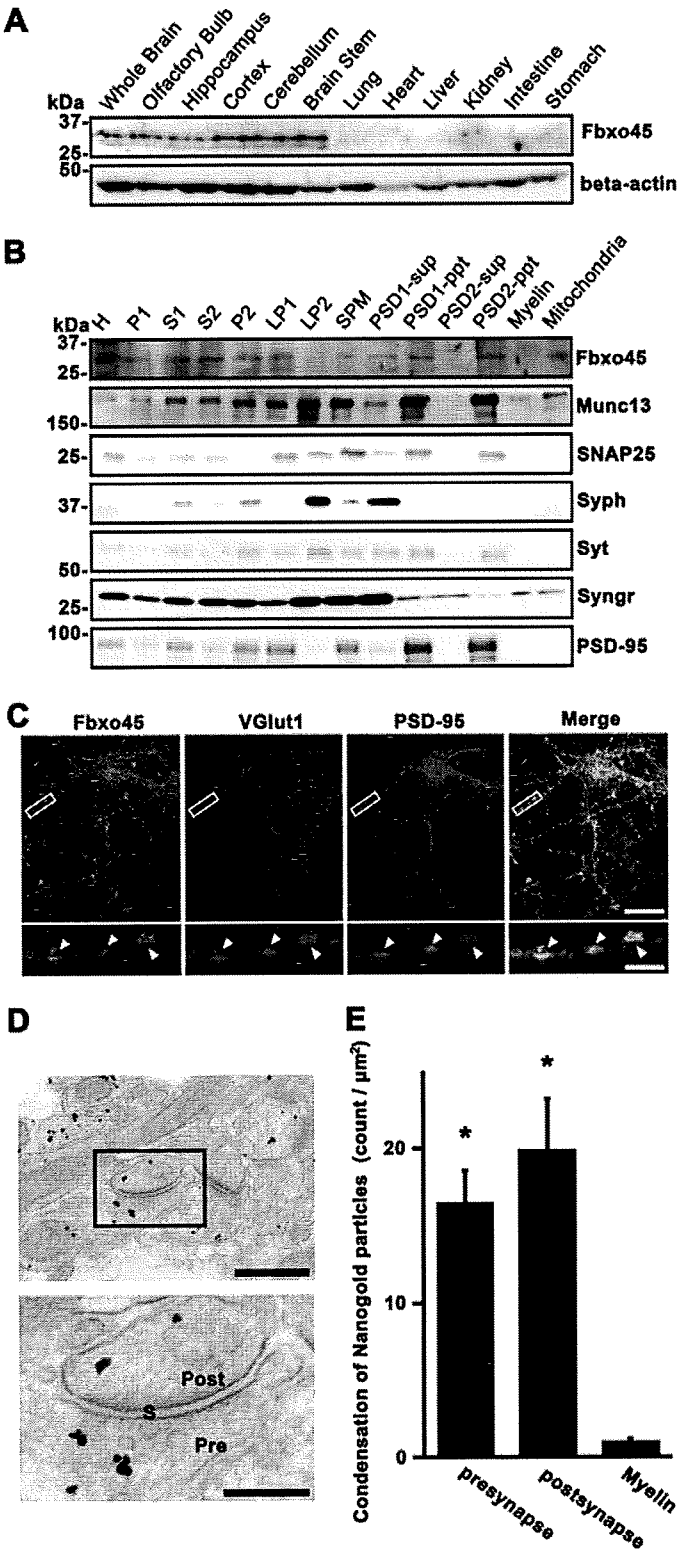

FIGURE 3. **Fbxo45 protein expression.** *A*, immunoblot analysis of Fbxo45 in adult mice is shown. *B*, subcellular distribution of Fbxo45 in the mouse brain is shown. Immunoblot analysis of Fbxo45, Munc13, SNAP25, synaptophysin (*Syph*), synaptotagmin (*Syt*), synaptogyrin (*Syngr*), or PSD-95 in the indicated fractions showed that Fbxo45 was enriched at the synaptic region, including the synaptosomal membrane fraction (*LP1*) and postsynaptic density (*PSD*). *H*, homogenate; *P1*, nuclear fraction; *S1*, crude synaptosomal fraction; *S2*, cytosolic synaptosomal fraction; *P2*, crude synaptosomal pellet fraction; *LP2*, synaptosomal vesicle fraction; *SPM*, synaptic plasma membrane fraction. *C*, immunocytochemistry of primary cultured rat hippocampal neurons expressing Fbxo45 is shown. Shown are Fbxo45 (*green*), VGlut1 (*red*), and PSD-95 (*purple*) (*upper panels*). Magnifications of the *boxed areas* in the *upper panels* are shown in the *lower panels*. *Arrowheads* indicate synapses, at which VGlut1 and PSD-95 were colocalized. *Scale bars*: 20 μm in the *upper panels*, 5 μm in the *lower panels*). *D*, shown is immunoelectron microscopy of endogenous Fbxo45. The *lower panel* shows a magnified image of the *boxed area* in the *upper panel*. *S*, synapse; *Pre*, presynaptic terminal; *Post*, postsynaptic terminal. *Scale bars*: 0.5 μm in the *upper panel*, 0.2 μm in the *lower panel*. *E*, localization of nanogold particles was quantitatively evaluated on each indicated structures (count/μm²). *Asterisk*, unpaired *t* test, $p < 0.01$.

ubiquitinated bands were detected in immunoprecipitates prepared from cells without FLAG-Fbxo45 (Fig. 5*B*). These results indicate that Fbxo45 indeed induced the ubiquitination.

Involvement of Fbxo45 in the Degradation of Munc13-1—The findings that Fbxo45 regulates mEPSC frequency and protein ubiquitination led us to speculate that Fbxo45 might control the degradation of a substrate in the nerve terminal to regulate neurotransmission. To find candidate substrates of Fbxo45, we first evaluated several synaptic proteins immunoprecipitated with Fbxo45. Munc13-1, the synaptic vesicle priming factor, was identified as one of Fbxo45-binding proteins. Moreover, we found that Munc13-1 interacted with the Fbxo45 deletion mutant (101–286 aa) that included the SPRY domain but not with deletion mutants lacking the SPRY domain (54–140 and 1–140 aa) (Fig. 6*A*).

To examine whether Fbxo45 affects the protein level of Munc13-1, we first co-expressed FLAG-Fbxo45 and Myc-Munc13-1 or Myc-RIM1 (rab3-interacting molecule 1), another vesicle priming factor in COS cells. With the expression of Fbxo45, the level of Munc13-1 decreased in a dose-dependent manner, but in sharp contrast the level of RIM1 did not change (Fig. 6*B*).

Next, to examine whether Fbxo45 affects the stability of Munc13-1, we co-transfected 293T cells with Munc13-1, Fbxo45, and Fbxo45 deletion mutants and then inhibited new protein synthesis by incubating the cells with cycloheximide for various times. The stability of Munc13-1 was assessed by immunoblotting analysis. The overexpression of Fbxo45 promoted a significantly faster degradation of Munc13-1 (half-life 4 h) compared with the control (Vec, Fbxo45 deletion mutants). In contrast, degradation of Munc13-1 was inhibited and rebuilt to control the level in Fbxo45-expressing cells treated with MG132 (Fig. 6*C*). The knockdown of Fbxo45 also showed delay of degradation of endogenous Munc13-1 (Fig. 6*D*). These results indicate that Fbxo45 interacts with Munc13-1 via SPRY domain and leads to degradation by UPS.

DISCUSSION

Information is passed from one neuron to the next by the release of neurotransmitters at the synapse. Neurotransmitter release is mediated by recycled neurotransmitter-containing synaptic vesicles at the presynaptic plasma membrane. A key event in neurotransmitter release is the priming step, which takes place before the fusion of a synaptic vesicle with the presynaptic active zone membrane. The priming step dramatically increases the propensity for vesicular release by lowering the energy barrier for fusion, thereby enabling the vesicles to use the action potential-induced transient Ca^{2+} increase efficiently for rapid exocytosis (46). Munc13-1 plays an essential role in

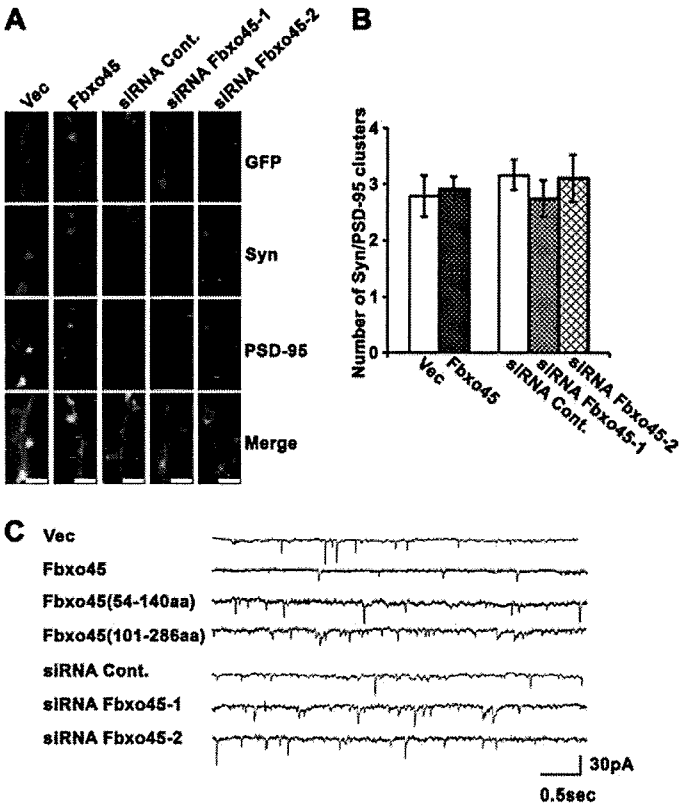

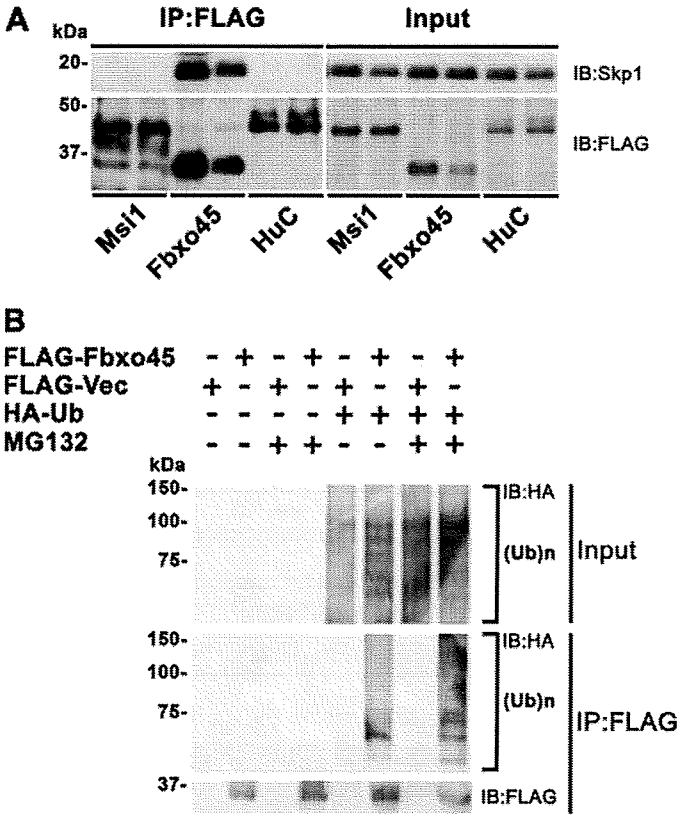

FIGURE 5. **Fbxo45 interacts with Skp1 and induces protein ubiquitination.** *A*, shown is an immunoprecipitation (*IP*) assay of FLAG-Fbxo45 with endogenous Skp1 compared with FLAG-Musashi1 (Msi1) or FLAG-HuC as a negative control. *IB*, immunoblot. *B*, shown is ubiquitination activity of Fbxo45 in 293T cells. The high molecular mass, ubiquitinated proteins are labeled *(Ub)n* at the *right*.

the neurotransmitter release machinery. In Munc13-1-deficient neurons, both spontaneous and evoked transmitter secretion are dramatically reduced, while vesicle docking to the active zone is essentially normal (47–50). On the other hand, the overexpression of Munc13-1 enhances neurotransmitter release at neuromuscular junctions in *Xenopus* (51). To control the level of Munc13-1 protein at synaptic sites, a spatially regulated protein degradation system like UPS is required. In support of this concept, the *Drosophila* Munc13-1 homologue DUNC13 is ubiquitinated, and it selectively accumulates in the

FIGURE 4. **Regulation of synaptic activity by Fbxo45.** *A*, shown is immunocytochemistry of cultured hippocampal neurons transfected with full-length of Fbxo45, vector control (*Vec*), siRNAs against Fbxo45 (*siRNA Fbxo45-1*, *siRNA Fbxo45-2*), or a control siRNA (*siRNA Cont.*) and EGFP. GFP (*green*), Synapsin-I (*Syn*; *red*), and PSD-95 (*white*) (scale *bars*: 5 μm). *B*, shown is quantification of the clusters that Synapsin-I and PSD-95 colocalized in the dendrites shown in *A*. *Vec*, $n = 18$; *Fbxo45*, $n = 29$; *siRNA control*, $n = 24$; siRNA Fbxo45-1, $n = 20$; *siRNA Fbxo45-2*, $n = 11$ dendrites. *C*, shown is a representative recording of the α-amino-3-hydroxy-5-methyl-4-isoxazolepropionate receptor-mediated mEPSC from neurons transfected with full-length or deletion mutants of Fbxo45, vector control, siRNAs against Fbxo45, or a control siRNA. *D*, quantification is shown of the mEPSC frequency and amplitude under the conditions described in *C*. *Vec*, $n = 11$; *Fbxo45*, $n = 9$; *Fbxo45(54–140aa)*, $n = 9$; *Fbxo45(101–286aa)*, $n = 9$; *siRNA control*, $n = 9$; *siRNA Fbxo45-1*, $n = 12$; *siRNA Fbxo45-2*, $n = 6$ neurons; *asterisk*, unpaired *t* test, $p < 0.05$). *E*, shown is mEPSC frequency in neurons transfected with Fbxo45 or the control vector in 2, 5, or 10 mM extracellular Ca^{2+}. (*Vec*, $n = 11, 14, 14$; *Fbxo45*, $n = 12, 8, 13$; *siRNA control*, $n = 9, 6, 7$; *siRNA Fbxo45-1*, $n = 12, 9, 8$; *siRNA Fbxo45-2*, $n = 6, 6, 7$ neurons (2, 5, 10 mM extracellular Ca^{2+}); *asterisk*, unpaired *t* test, $p < 0.05$.

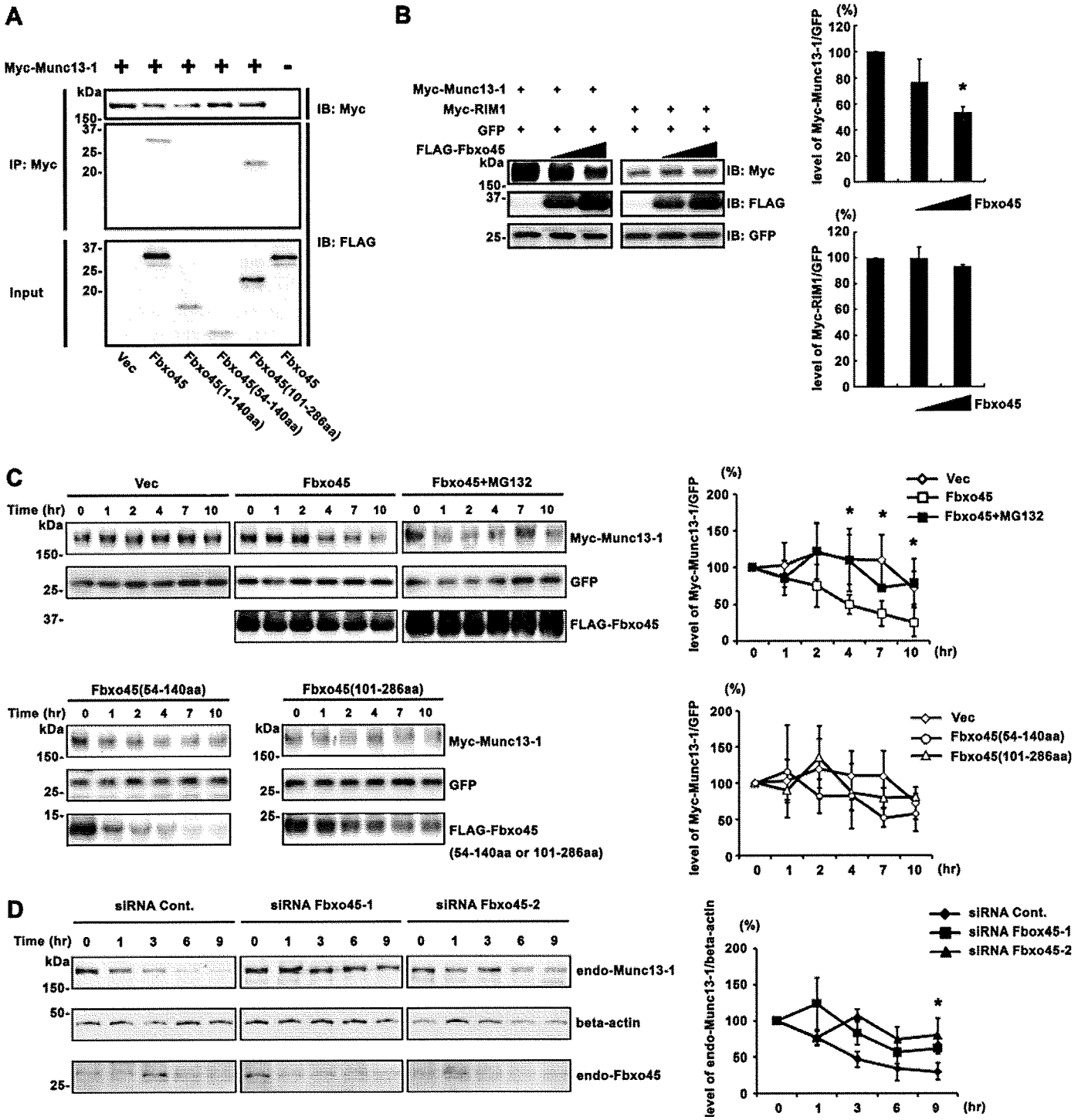

FIGURE 6. **Involvement of Fbxo45 in the degradation of Munc13-1.** *A*, Fbxo45 interacts with Munc13-1 through the SPRY domain. FLAG-tagged full-length or deletion mutants of Fbxo45 were co-expressed with Myc-Munc13-1 in 293T cells and then immunoprecipitated (*IP*) with an anti-Myc antibody. The precipitates were analyzed by immunoblotting (*IB*) using an anti-FLAG or anti-Myc antibody. *Vec*, vector. *B*, the level of Munc13-1 protein was decreased by Fbxo45 in a dose-dependent manner. In contrast, the RIM1 level was not affected by Fbxo45. Shown is quantification of the optical densities of the Munc13-1 and RIM1 bands. The protein levels, normalized to those of the corresponding EGFP bands, are shown as a percentage of the normalized value without Fbxo45 co-expression. *Asterisk*, $p < 0.05$, Mann-Whitney *U* test. *C*, shown is regulation of Munc13-1 stability by Fbxo45. Munc13-1 was co-expressed with Fbxo45 full-length, Fbxo45 deletion mutants, or Fbxo45 with MG132 and EGFP in 293T cells. *D*, shown is regulation of endogenous Munc13-1 protein stability by endogenous Fbxo45 in Neuro2A cells. siRNA control or siRNAs against Fbxo45 were transfected into Neuro2A cell. The protein stability was assessed by immunoblot analysis after incubation with cycloheximide for various times. Protein decay curves were determined from these studies. The optical density of the Munc13-1 or endogenous Munc13-1 bands was normalized to that of the corresponding EGFP or β-actin band, respectively, and is shown as a percentage of the normalized value for the 0-h time point. *Asterisk*, $p < 0.05$. Mann-Whitney *U* test.

presynaptic terminal after proteasome inhibition (52), although the E3 for DUNC13 is still unknown.

In the present study we cloned and identified the *Fbxo45* gene, which encodes an F-box ubiquitin ligase that is specifically expressed in the nervous system. Our newly generated anti-Fbxo45 antibody demonstrated the synaptic localization of Fbxo45. Subcellular distribution assay showed that Fbxo45 expression overlapped with presynaptic protein Munc13 in LP1, synaptic plasma membrane fraction, and PSD. Fbxo45 functions as a ubiquitin ligase of vesicle-priming factor Munc13-1 and regulated the spontaneous mEPSC activity in mature neurons. Munc13-1-deficient mice have been shown to exhibit a decrease of mEPSC frequency (53), which was almost same quantitative changes as overexpression of Fbxo45. Furthermore, we showed that the level of the Munc13-1 was regulated by Fbxo45, suggesting that Fbxo45 is critically involved in the regulation of synaptic activity and functions by controlling Munc13-1 protein via ubiquitin dependent proteolysis. It remains to be studied whether there are additional substrates of Fbxo45 involved in the regulation of synaptic activity at the postsynaptic site, because Fbxo45 expresses at not only the presynaptic but also the postsynaptic site.

Fbxo45 is highly conserved among species from *C. elegans* to mammals. The Fbxo45 homologues FSN-1 (*C. elegans*) and DFsn (*Drosophila*) have been shown to be important for synapse formation in the presynaptic neurons by interacting with RING finger-type E3 RPM-1 (*C. elegans*) and Highwire (*Drosophila*), respectively (43, 54). Details on the interaction between Fbxo45 and PAM (protein associated with Myc), RPM-1/Highwire mammalian homologue, will be described elsewhere (45). The *fsn-1* mutant in *C. elegans* and the *DFsn* mutant in *Drosophila* exhibit increased numbers of synapses and abnormal transmission at the neuromuscular junction. *fsn-1*-null animals also exhibit enhanced levels of a receptor-tyrosine kinase, anaplastic lymphoma kinase (ALK), and their phenotype is suppressed by mutations in ALK, suggesting that FSN-1 contributes to the stabilization of synapse formation through a protein degradation pathway (43). In *Drosophila*, DFsn down-regulates the levels of a MAP kinase kinase kinase, Wallenda/dual leucine zipper kinase (DLK), and restrains the growth of synaptic terminals (54). These findings indicate that FSN-1 and DFsn are required for synaptic growth in developing neurons. However, the role of DFsn/FSN-1 in mature neurons is still unclear. Here we showed that Fbxo45 negatively regulated neurotransmission without affecting synapse formation in mature hippocampal neurons. This difference may be because of context-dependent functions of Fbxo45/DFsn/FSN-1 in addition to differences in the species and neuronal regions examined (*i.e.* the hippocampus *versus* the neuromuscular junction). That is, the roles of Fbxo45/DFsn/FSN-1 might switch from those regulating synapse formation to those regulating neurotransmission as the development of the nervous system progresses.

The UPS has recently emerged as an important mechanism for regulating synaptic function. Several ubiquitin ligases are known to regulate presynaptic protein turnover and synaptic efficacy. For example, the E3 ligase SCRAPPER ubiquitinates and mediates the proteasomal degradation of RIM1, a vesicle-priming protein located in the presynaptic active zone. In *Scrapper* knock-out mice, the RIM1 protein levels have an increased half-life, and the mice exhibit enhanced mEPSC frequency. These results indicate that SCRAPPER regulates presynaptic transmitter release by targeting RIM1 for degradation through the UPS (9).

Interestingly, the levels of other presynaptic proteins, including Munc13-1, are also elevated in *Scrapper*-knock-out mice and/or reduced upon SCRAPPER overexpression. However, there is no direct interaction between SCRAPPER and Munc13-1. Therefore, other factors, like the Fbxo45 pathway, appear to regulate the amount of Munc13-1 protein and Munc13-1-dependent neurotransmitter release. A bidirectional pathway between Fbxo45-Munc13-1 and SCRAPPER-RIM1 may cooperatively regulate the priming step of synaptic vesicle release by protein degradation to modulate synaptic transmission. Therefore, an impairment in this pathway may lead to dysfunctional neurotransmission and disruptions in neuronal communication.

Acknowledgments—We thank Dr. M. Matsumoto, Dr. T. Nagai, Dr. M. Watanabe, Dr. M. Uchigashima, Dr. K. O'Donovan, Dr. M. Sakaguchi, Dr. T. Iijima, Dr. M. Yano, Dr. H. Kawahara, Dr. S. Fukami, K. Yasutake, and our colleagues in the Okano, Setou, and Takahashi laboratories for help, encouragement, and advice, K. Tada, R. Tada, and N. Tada for critical advice and continuous support, and Dr. K. Tanaka for valuable reagents.

REFERENCES

1. Li, L., and Chin, L. S. (2003) *Cell. Mol. Life Sci.* **60,** 942–960
2. Sudhof, T. C. (2004) *Annu. Rev. Neurosci.* **27,** 509–547
3. Südhof, T. C. (2008) *Nature* **455,** 903–911
4. Südhof, T. C., and Malenka, R. C. (2008) *Neuron.* **60,** 469–476
5. Inoue, E., Mochida, S., Takagi, H., Higa, S., Deguchi-Tawarada, M., Takao-Rikitsu, E., Inoue, M., Yao, I., Takeuchi, K., Kitajima, I., Setou, M., Ohtsuka, T., and Takai, Y. (2006) *Neuron.* **50,** 261–275
6. DiAntonio, A., and Hicke, L. (2004) *Annu. Rev. Neurosci.* **27,** 223–246
7. Yi, J. J., and Ehlers, M. D. (2005) *Neuron.* **47,** 629–632
8. Yi, J. J., and Ehlers, M. D. (2007) *Pharmacol. Rev.* **59,** 14–39
9. Yao, I., Takagi, H., Ageta, H., Kahyo, T., Sato, S., Hatanaka, K., Fukuda, Y., Chiba, T., Morone, N., Yuasa, S., Inokuchi, K., Ohtsuka, T., Macgregor, G. R., Tanaka, K., and Setou, M. (2007) *Cell* **130,** 943–957
10. Hershko, A., and Ciechanover, A. (1998) *Annu. Rev. Biochem.* **67,** 425–479
11. Voges, D., Zwickl, P., and Baumeister, W. (1999) *Annu. Rev. Biochem.* **68,** 1015–1068
12. Hershko, A., Ciechanover, A., and Varshavsky, A. (2000) *Nat. Med.* **6,** 1073–1081
13. Pickart, C. M. (2001) *Annu. Rev. Biochem.* **70,** 503–533
14. Nakayama, K. I., and Nakayama, K. (2006) *Nat. Rev. Cancer* **6,** 369–381
15. Bai, C., Sen, P., Hofmann, K., Ma, L., Goebl, M., Harper, J. W., and Elledge, S. J. (1996) *Cell* **86,** 263–274
16. Schulman, B. A., Carrano, A. C., Jeffrey, P. D., Bowen, Z., Kinnucan, E. R., Finnin, M. S., Elledge, S. J., Harper, J. W., Pagano, M., and Pavletich, N. P. (2000) *Nature* **408,** 381–386
17. Hatakeyama, S., Kitagawa, M., Nakayama, K., Shirane, M., Matsumoto, M., Hattori, K., Higashi, H., Nakano, H., Okumura, K., Onoé, K., Good, R. A., and Nakayama, K. (1999) *Proc. Natl. Acad. Sci. U.S.A.* **96,** 3859–3863
18. Kitagawa, M., Hatakeyama, S., Shirane, M., Matsumoto, M., Ishida, N., Hattori, K., Nakamichi, I., Kikuchi, A., Nakayama, K., and Nakayama, K. (1999) *EMBO J.* **18,** 2401–2410

19. Nakayama, K. I., and Nakayama, K. (2005) *Semin. Cell Dev. Biol.* **16,** 323–333
20. DiAntonio, A., Haghighi, A. P., Portman, S. L., Lee, J. D., Amaranto, A. M., and Goodman, C. S. (2001) *Nature* **412,** 449–452
21. Schaefer, A. M., Hadwiger, G. D., and Nonet, M. L. (2000) *Neuron.* **26,** 345–356
22. Wan, H. I., DiAntonio, A., Fetter, R. D., Bergstrom, K., Strauss, R., and Goodman, C. S. (2000) *Neuron.* **26,** 313–329
23. Zhen, M., Huang, X., Bamber, B., and Jin, Y. (2000) *Neuron.* **26,** 331–343
24. Kurihara, T., Ozawa, Y., Nagai, N., Shinoda, K., Noda, K., Imamura, Y., Tsubota, K., Okano, H., Oike, Y., and Ishida, S. (2008) *Diabetes* **57,** 2191–2198
25. Wheeler, T. C., Chin, L. S., Li, Y., Roudabush, F. L., and Li, L. (2002) *J. Biol. Chem.* **277,** 10273–10282
26. Chin, L. S., Vavalle, J. P., and Li, L. (2002) *J. Biol. Chem.* **277,** 35071–35079
27. Helton, T. D., Otsuka, T., Lee, M. C., Mu, Y., and Ehlers, M. D. (2008) *Proc. Natl. Acad. Sci. U.S.A.* **105,** 19492–19497
28. Haas, K. F., and Broadie, K. (2008) *Biochim. Biophys. Acta* **1779,** 495–506
29. Darnell, R. B., and Posner, J. B. (2003) *N. Engl. J. Med.* **349,** 1543–1554
30. Musunuru, K., and Darnell, R. B. (2001) *Annu. Rev. Neurosci.* **24,** 239–262
31. Imai, T., Tokunaga, A., Yoshida, T., Hashimoto, M., Mikoshiba, K., Weinmaster, G., Nakafuku, M., and Okano, H. (2001) *Mol. Cell. Biol.* **21,** 3888–3900
32. Sato, S., Chiba, T., Sakata, E., Kato, K., Mizuno, Y., Hattori, N., and Tanaka, K. (2006) *EMBO J.* **25,** 211–221
33. Oshikawa, K., Matsumoto, M., Yada, M., Kamura, T., Hatakeyama, S., and Nakayama, K. I. (2003) *Biochem. Biophys. Res. Commun.* **303,** 1209–1216
34. Akamatsu, W., Okano, H. J., Osumi, N., Inoue, T., Nakamura, S., Sakakibara, S., Miura, M., Matsuo, N., Darnell, R. B., and Okano, H. (1999) *Proc. Natl. Acad. Sci. U.S.A.* **96,** 9885–9890
35. Fukaya, M., Uchigashima, M., Nomura, S., Hasegawa, Y., Kikuchi, H., and Watanabe, M. (2008) *Eur. J. Neurosci.* **28,** 1744–1759
36. Hennou, S., Kato, A., Schneider, E. M., Lundstrom, K., Gähwiler, B. H., Inokuchi, K., Gerber, U., and Ehrengruber, M. U. (2003) *Eur. J. Neurosci.* **18,** 811–819
37. Yano, M., Okano, H. J., and Okano, H. (2005) *J. Biol. Chem.* **280,** 12690–12699
38. Yao, I., Hata, Y., Ide, N., Hirao, K., Deguchi, M., Nishioka, H., Mizoguchi, A., and Takai, Y. (1999) *J. Biol. Chem.* **274,** 11889–11896
39. Yao, I., Hata, Y., Hirao, K., Deguchi, M., Ide, N., Takeuchi, M., and Takai, Y. (1999) *J. Biol. Chem.* **274,** 27463–27466
40. Jin, J., Cardozo, T., Lovering, R. C., Elledge, S. J., Pagano, M., and Harper, J. W. (2004) *Genes Dev.* **18,** 2573–2580
41. Yoshida, K. (2005) *Oncol. Rep.* **14,** 531–535
42. Ponting, C., Schultz, J., and Bork, P. (1997) *Trends Biochem. Sci.* **22,** 193–194
43. Liao, E. H., Hung, W., Abrams, B., and Zhen, M. (2004) *Nature* **430,** 345–350
44. Sakakibara, S., Imai, T., Hamaguchi, K., Okabe, M., Aruga, J., Nakajima, K., Yasutomi, D., Nagata, T., Kurihara, Y., Uesugi, S., Miyata, T., Ogawa, M., Mikoshiba, K., and Okano, H. (1996) *Dev. Biol.* **176,** 230–242
45. Saiga, T., Fukuda, T., Matsumoto, M., Tada, H., Okano, H. J., Okano, H., and Nakayama, K. I. (2009) *Mol. Cell. Biol.* **29,** 3529–3543
46. Rosenmund, C., and Stevens, C. F. (1996) *Neuron.* **16,** 1197–1207
47. Aravamudan, B., Fergestad, T., Davis, W. S., Rodesch, C. K., and Broadie, K. (1999) *Nat. Neurosci.* **2,** 965–971
48. Augustin, I., Rosenmund, C., Südhof, T. C., and Brose, N. (1999) *Nature* **400,** 457–461
49. Richmond, J. E., Weimer, R. M., and Jorgensen, E. M. (2001) *Nature* **412,** 338–341
50. Varoqueaux, F., Sigler, A., Rhee, J. S., Brose, N., Enk, C., Reim, K., and Rosenmund, C. (2002) *Proc. Natl. Acad. Sci. U.S.A.* **99,** 9037–9042
51. Betz, A., Ashery, U., Rickmann, M., Augustin, I., Neher, E., Südhof, T. C., Rettig, J., and Brose, N. (1998) *Neuron.* **21,** 123–136
52. Speese, S. D., Trotta, N., Rodesch, C. K., Aravamudan, B., and Broadie, K. (2003) *Curr. Biol.* **13,** 899–910
53. Deák, F., Liu, X., Khvotchev, M., Li, G., Kavalali, E. T., Sugita, S., and Südhof, T. C. (2009) *J. Neurosci.* **29,** 8639–8648
54. Wu, C., Daniels, R. W., and DiAntonio, A. (2007) *Neural Dev.* **2,** 16
55. Sakakibara, S., Nakamura, Y., Satoh, H., and Okano, H. (2001) *J. Neurosci.* **21,** 8091–8107

nature genetics

Skp2 is required for survival of aberrantly proliferating *Rb1*-deficient cells and for tumorigenesis in $Rb1^{+/-}$ mice

Hongbo Wang[1,6], Frederick Bauzon[1,7], Peng Ji[1,6,7], Xiaoliang Xu[2,6,7], Daqian Sun[1], Joseph Locker[3], Rani S Sellers[3], Keiko Nakayama[4], Keiich I Nakayama[5], David Cobrinik[2,6] & Liang Zhu[1]

Heterozygosity of the retinoblastoma gene *Rb1* elicits tumorigenesis in susceptible tissues following spontaneous loss of the remaining functional allele. Inactivation of previously studied retinoblastoma protein (pRb) targets partially inhibited tumorigenesis in $Rb1^{+/-}$ mice[1–6]. Here we report that inactivation of pRb target Skp2 (refs. 7,8) completely prevents spontaneous tumorigenesis in $Rb1^{+/-}$ mice. Targeted *Rb1* deletion in melanotrophs ablates the entire pituitary intermediate lobe when Skp2 is inactivated. Skp2 inactivation does not inhibit aberrant proliferation of *Rb1*-deleted melanotrophs but induces their apoptotic death. Eliminating p27 phosphorylation on T187 in p27T187A knock-in mice reproduces the effects of *Skp2* knockout, identifying p27 ubiquitination by SCF^{Skp2} ubiquitin ligase as the underlying mechanism for Skp2's essential tumorigenic role in this setting. *RB1*-deficient human retinoblastoma cells also undergo apoptosis after Skp2 knockdown; and ectopic expression of p27, especially the p27T187A mutant, induces apoptosis. These results reveal that *Skp2* becomes an essential survival gene when susceptible cells incur *Rb1* deficiency.

Skp2 binds T187-phosphorylated p27 for the SCF^{Skp2} ubiquitin ligase to ubiquitinate p27 (ref. 9). pRb binds Skp2 to interfere this binding and ubiquitination[7]. pRb-Skp2 binding also bridges Skp2 to the APC-Cdh1 ubiquitin ligase for Skp2 ubiquitination[8]. Because Skp2 is a target for the transcription factor E2F (refs. 10,11), pRb could repress Skp2 mRNA expression via E2F. Consistent with the above findings, $Rb1^{+/-}$ mice developed $Rb1^{-/-}$ pituitary tumors that had substantially increased amounts of Skp2 mRNA and protein along with decreased amounts of p27 protein (**Fig. 1a,b**).

To define the role of Skp2 in tumorigenesis in $Rb1^{+/-}$ mice, we generated cohorts of $Rb1^{+/-}Skp2^{+/+}$ and $Rb1^{+/-}Skp2^{-/-}$ mice. Skp2 is not required for pituitary gland development (see **Supplementary Fig. 1**). $Rb1^{+/-}$ mice develop pituitary intermediate lobe melanotroph tumors with a well-defined course, from early atypical proliferates to foci, microscopic tumors and gross tumors (**Supplementary Fig. 2a**), resulting in death around 1 year of age[12]. At 6 months more than half of $Rb1^{+/-}Skp2^{+/+}$ mice had early atypical proliferates and foci (**Fig. 1c**). By 9 months one pituitary had a gross tumor, and most had foci and microscopic tumors. Later, all 27 $Rb1^{+/-}Skp2^{+/+}$ mice died between 10 and 15 months of age (**Fig. 1d**), all but one with gross pituitary tumors (**Fig. 1c**). In contrast, none of the $Rb1^{+/-}Skp2^{-/-}$ mice had any sign of pituitary tumorigenesis at 6, 9 and 17 months, when healthy $Rb1^{+/-}Skp2^{-/-}$ mice were killed.

Thyroid C-cell tumors develop with 50–70% penetrance in $Rb1^{+/-}$ mice. Among the same 27 $Rb1^{+/-}Skp2^{+/+}$ mice, 16 had gross thyroid tumors at death, and the dead mouse that lacked a pituitary tumor had an especially large thyroid tumor (**Fig. 1c**). About half of the remaining dead mice had microscopic thyroid tumors (**Fig. 1c** and **Supplementary Fig. 2b**). In contrast, all 29 $Rb1^{+/-}Skp2^{-/-}$ mice had normal-appearing, tumor-free thyroid glands (**Fig. 1c**). Together with the lack of pituitary tumors, these results identify Skp2 as the first pRb target that is required for spontaneous tumorigenesis in $Rb1^{+/-}$ mice.

The above findings could reflect the fact that Skp2 plays a required role in the development of *Rb1* mutant tumors or that Skp2 is generally required for tumorigenesis. To begin to investigate these possibilities, we treated $Skp2^{+/+}$ and $Skp2^{-/-}$ mice with a tumorigenesis protocol using *N*-ethyl-*N*-nitrosurea (ENU) induction. This experiment demonstrated no difference in tumor development in the two genotypes, including survival (**Fig. 1e**) and tumor types and burdens (**Supplementary Fig. 3a**). Although Skp2 was frequently overexpressed in the tumors, its expression levels did not correlate with p27 protein levels (**Supplementary Fig. 3b**). Thus, Skp2 is not required for ENU-induced tumorigenesis.

Because spontaneous tumorigenesis in $Rb1^{+/-}$ mice requires the loss of the remaining *Rb1* allele, it was possible that *Skp2* inactivation prevented the second *Rb1* mutation, rather than the growth of *Rb1*-deficient tumors. We next used a tissue-specific *Rb1* deletion

[1]Department of Developmental and Molecular Biology and Medicine, The Albert Einstein Comprehensive Cancer Center and Liver Research Center, Albert Einstein College of Medicine, Bronx, New York, USA. [2]Dyson Vision Research Institute, Weill-Cornell Medical College, New York, New York, USA. [3]Department of Pathology, The Albert Einstein Comprehensive Cancer Center and Liver Research Center, Albert Einstein College of Medicine, Bronx, New York, USA. [4]Department of Functional Genomics, Division of Developmental Genetics, Tohoku University Graduate School of Medicine, Sendai, Japan. [5]Department of Molecular and Cellular Biology, Medical Institute of Bioregulation, Kyushu University, Fukuoka, Japan. [6]Present addresses: Whitehead Institute for Biomedical Research, Cambridge, Massachusetts, USA (P.J.); Peptide Binding Laboratory, The Salk Institute, La Jolla, California, USA (H.W.); Departments of Pathology (X.X.) and Pediatrics (D.C.), Memorial Sloan-Kettering Cancer Center, New York, New York, USA. [7]These authors contributed equally to this work and are listed alphabetically. Correspondence should be addressed to L.Z. (liang.zhu@einstein.yu.edu).

Received 19 June; accepted 28 October; published online 6 December 2009; doi:10.1038/ng.498

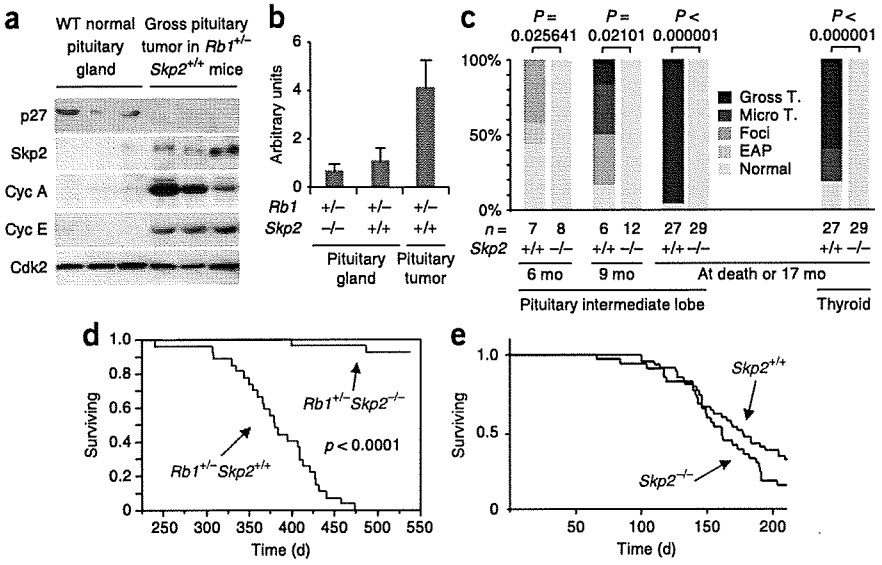

Figure 1 Roles of *Skp2* in spontaneous tumorigenesis in *Rb1*$^{+/-}$ mice and in ENU-induced tumorigenesis. (**a**) Expression of the indicated proteins in wild-type (WT) normal pituitary glands and pituitary tumors developed in *Rb1*$^{+/-}$*Skp2*$^{+/+}$ mice, determined by protein blot. (**b**) Amounts of Skp2 mRNA in pituitary glands and pituitary tumors (developed in *Rb1*$^{+/-}$ mice), determined by quantitative PCR (Q-PCR) normalized to the abundance of the enzyme GAPDH. (**c**) Incidence of pituitary and thyroid tumors at various stages in *Rb1*$^{+/-}$*Skp2*$^{+/+}$ and *Rb1*$^{+/-}$*Skp2*$^{-/-}$ mice. *P* values are by Fisher's exact tests (various lesions were combined for analyses). (**d**) Kaplan-Meier survival analysis for the indicated mice. *P* value is by log rank test. One *Rb1*$^{+/-}$*Skp2*$^{-/-}$ mouse died at 13 months, and one died at 16 months with macroscopically normal pituitary and thyroid glands. The causes of death were unclear, with a possible association with eye and skin lesions. (**e**) Kaplan-Meier survival analysis for the indicated mice treated with ENU.

scheme involving a proopiomelanocortin promoter–Cre recombinase (POMC-Cre) fusion and *loxP* sites to artificially generate *Rb1*$^{-/-}$ pituitary intermediate lobe melanotrophs[13]. To determine whether *Skp2* inactivation affects the efficiency of POMC-Cre–*loxP*-mediated recombination, we generated *POMC-Cre;Rosa26R;Skp2*$^{+/+}$ and *POMC-Cre;Rosa26R;Skp2*$^{-/-}$ mice. We found that the *POMC-Cre* strain could induce Cre-*loxP*–mediated deletion in most of the intermediate lobe melanotrophs in both *Skp2*$^{+/+}$ and *Skp2*$^{-/-}$ mice (**Fig. 2a**). Because the POMC promoter is also active in corticotrophs in the anterior lobe, scattered anterior lobe recombination events were detected in both strains of mice as well (**Fig. 2a, v,vi**).

We then generated *POMC-Cre;Rb1*$^{lox/lox}$*Skp2*$^{+/+}$ and *POMC-Cre;Rb1*$^{lox/lox}$*Skp2*$^{-/-}$ mice and examined their pituitary glands at 7 weeks of age. As expected[13], *POMC-Cre;Rb1*$^{lox/lox}$*Skp2*$^{+/+}$ mice harbored dysplastic nodular lesions across the entire intermediate lobes (**Fig. 2b, ii,vi**). Unexpectedly, *POMC-Cre;Rb1*$^{lox/lox}$*Skp2*$^{-/-}$ mice did not contain normal-appearing intermediate lobes as we predicted based on the lack of pituitary tumorigenesis in *Rb1*$^{+/-}$*Skp2*$^{-/-}$ mice. Instead, the intermediate lobes of these mice were essentially absent, with only a single layer of lining cells separating the anterior and posterior lobes (**Fig. 2b, iii,vii**). The intermediate lobes of *POMC-Cre;Rb1*$^{lox/lox}$*Skp2*$^{+/-}$ mice were also considerably thinner than normal (**Fig. 2b, iv,viii**). These results confirm that *Skp2* inactivation blocks tumorigenesis and demonstrate that this effect was achieved not by reverting *Rb1*-deficient melanotrophs to normal cells but by eliminating them.

We traced the fate of *Rb1* and *Skp2* doubly deficient melanotrophs by generating *POMC-Cre;Rosa26R;Rb1*$^{lox/lox}$*Skp2*$^{+/+}$ and *POMC-Cre;Rosa26R;Rb1*$^{lox/lox}$*Skp2*$^{-/-}$ mice and allowing them to age to 10–13 weeks. The intermediate lobes of *POMC-Cre;Rosa26R;Rb1*$^{lox/lox}$ *Skp2*$^{+/+}$ mice, observed with hematoxylin stain and enhanced yellow fluorescent protein (EYFP) fluorescence (**Fig. 2c, i,iii**), were in more advanced stages of tumorigenesis than those at 7 weeks (compare with **Fig. 2b, ii**), whereas the intermediate lobes of *POMC-Cre;Rosa26R;Rb1*$^{lox/lox}$*Skp2*$^{-/-}$ mice remained a single-cell layer (**Fig. 2c, ii**). Notably, the cells in this layer were EYFP positive (**Fig. 2c, iv**), suggesting that this single-cell layer environment could prevent death of *Rb1* and *Skp2* doubly deficient cells or that these cells escaped

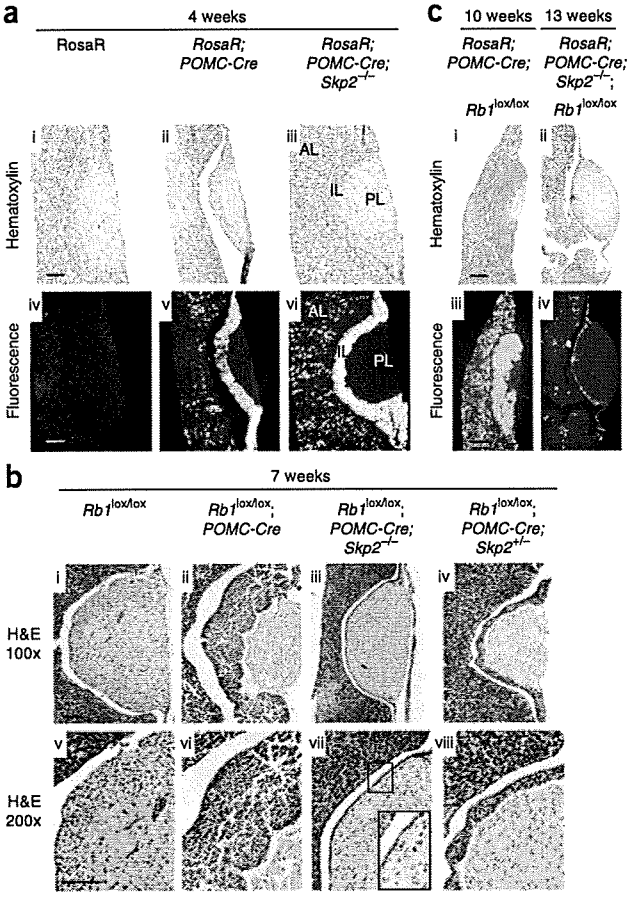

Figure 2 Effects of targeted deletion of *Rb1* in pituitary intermediate and anterior lobes of *Skp2*$^{+/+}$ and *Skp2*$^{-/-}$ mice. (**a**) The *POMC-Cre* strain induced Cre-*loxP*–mediated excision in posterior and anterior lobes of *Skp2*$^{+/+}$ and *Skp2*$^{-/-}$ mice. '*Rosa26R*' indicates *Rosa26-loxP*-STOP-*loxP-EYFP*. Mice were examined at 4 weeks of age. EYFP expression was by fluorescence of frozen-sectioned samples. (**b**) Pituitary intermediate lobes of indicated mice at 7 weeks of age. Hematoxylin and eosin (H&E)-stained sections of various pituitaries are shown. Large inset in **vii** is enlarged view of areas marked by the small box. (**c**) Pituitary glands of the indicated mice at the indicated ages, examined as in **a**. Scale bar, 200 μm.

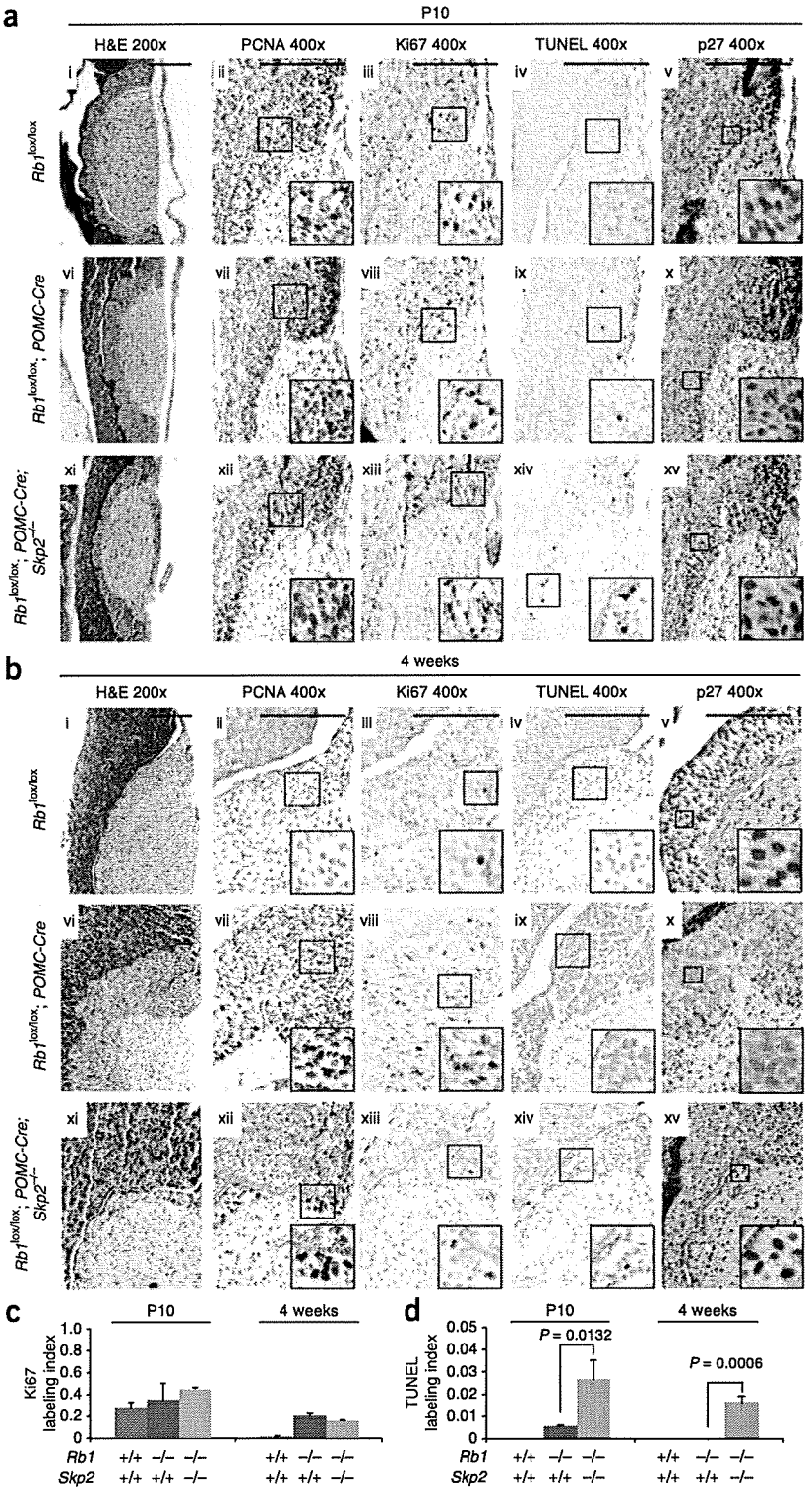

Figure 3 Effects of Skp2 inactivation on E2F deregulation, aberrant proliferation and apoptosis, and p27 expression in pituitary intermediate lobes following *Rb1* deletion. (**a**,**b**) Various indicated mice at the ages of P10 (**a**) and 4 weeks (**b**) are presented. E2F deregulation is examined by PCNA expression, proliferation by Ki67 expression and apoptosis by TUNEL labeling. (**c**,**d**) Quantification of Ki67 (**c**) and TUNEL labeling (**d**) in intermediate lobes was performed with three pituitaries of each indicated genotype at the indicated ages. *Rb1* genotypes indicate the outcome of Cre-*loxP*–mediated deletion in intermediate lobe. *P* values are by Student's *t*-test. Error bars, s.d. Scale bar, 200 μm.

Rb1 deletion. We also found that *Rb1* deletion in corticotrophs induced the presence of more corticotrophs in the anterior lobe, and combined deletion of *Rb1*and *Skp2* markedly reduced their numbers (**Fig. 2a, v,vi,** and **c, iii,iv**). This indicates that combined *Rb1* and *Skp2* deletion could eliminate corticotrophs as well as melanotrophs.

We next harvested the mice at earlier ages to investigate how the intermediate lobes were eliminated (**Fig. 3**). At postnatal day (P) 10 the intermediate lobes of both *POMC-Cre;Rb1*$^{lox/lox}$ *Skp2*$^{+/+}$ and *POMC-Cre;Rb1*$^{lox/lox}$*Skp2*$^{-/-}$ mice showed slightly higher cellularity than those of *Rb1*$^{lox/lox}$ mice (**Fig. 3a, i,vi,xi,** and data not shown). Expression of PCNA (encoded by an E2F target gene) and Ki67 (a proliferation marker) was readily observed in *Rb1*$^{lox/lox}$ melanotrophs, indicating the proliferative status of these cells at this age (**Fig. 3a, ii,iii,** and **c**). Deletion of *Rb1* increased PCNA and Ki67 expression, consistent with deregulation of E2F and proliferation caused by pRb inactivation (**Fig. 3a, vii,viii,** and **c**). *Skp2* inactivation reduced neither PCNA expression nor the aberrant proliferation of the *Rb1*-deficient cells (**Fig. 3a, xii,xiii,** and **c**), but it significantly increased TUNEL-positive intermediate lobe cells compared with *Rb1*$^{lox/lox}$ and *POMC-Cre;Rb1*$^{lox/lox}$ *Skp2*$^{+/+}$ controls (**Fig. 3a, iv,ix,xiv,** and **d**).

At 4 weeks of age the cells in the intermediate lobes of *POMC-Cre;Rb1*$^{lox/lox}$*Skp2*$^{-/-}$ mice maintained deregulated PCNA expression and proliferation and increased apoptosis (**Fig. 3b–d**). Whereas the aberrantly proliferating intermediate lobes of 4-week-old *POMC-Cre;Rb1*$^{lox/lox}$*Skp2*$^{+/+}$ mice had become more than twofold thicker than those of the *Rb1*$^{lox/lox}$ controls (**Fig. 3b, i,vi**), the proliferating yet apoptotic intermediate lobes of 4-week-old *POMC-Cre;Rb1*$^{lox/lox}$ *Skp2*$^{-/-}$ mice had become more than twofold thinner than normal (**Fig. 3b, xi**). Together, these findings indicate that *Skp2* is required for the survival of aberrantly proliferating *Rb1*-deficient melanotrophs and that *Rb1*$^{-/-}$*Skp2*$^{-/-}$ melanotroph apoptosis caused the elimination of the intermediate lobes in *POMC-Cre;Rb1*$^{lox/lox}$*Skp2*$^{-/-}$ mice.

POMC-Cre;Rb1$^{lox/lox}$ mice allowed us to evaluate the effect of Skp2 on p27 expression during melanotroph tumorigenesis using immunohistochemical staining. Melanotrophs of *Rb1*$^{lox/lox}$, *POMC-Cre;Rb1*$^{lox/lox}$ and *POMC-Cre;Rb1*$^{lox/lox}$*Skp2*$^{-/-}$ mice at P10 had comparable nuclear p27 protein stains (**Fig. 3a, v,x,xv**). However, by 4 weeks p27 concentrations clearly decreased in melanotrophs of *POMC-Cre;Rb1*$^{lox/lox}$ mice (**Fig. 3b, x**) but were maintained in the melanotrophs of *POMC-Cre;Rb1*$^{lox/lox}$*Skp2*$^{-/-}$ mice (**Fig. 3b, xv**),

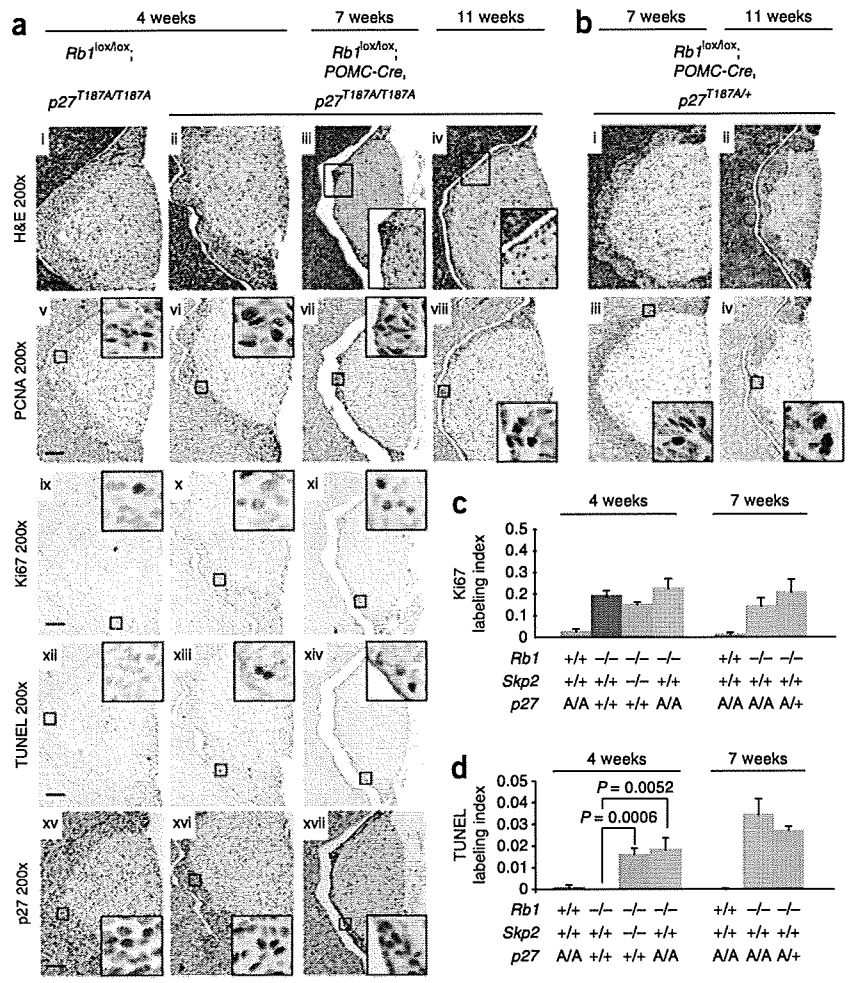

Figure 4 Effects of targeted deletion of *Rb1* in pituitary intermediate lobe of p27T187A knock-in mice. (**a**) Intermediate lobe morphology, PCNA expression, Ki67 and TUNEL labeling, and p27 expression were examined at the indicated ages. (**b**) Intermediate lobe morphology and PCNA expression after *Rb1* deletion in $p27^{T187A/+}$ mice at 7 and 11 weeks of age. (**c**,**d**) Quantification of Ki67 (**c**) and TUNEL labeling (**d**) in **a**. *P* values are by Student's *t*-test. Error bars, s.d. Scale bar, 200 μm.

suggesting that *Skp2* is required for the downregulation of p27 during melanotroph tumorigenesis following *Rb1* deletion.

We next investigated how Skp2 inactivation led to the failure of p27 downregulation and whether this failure was responsible for the tumor-blocking effects of Skp2 inactivation. *In vitro* studies have established that Skp2 mediates p27 ubiquitination in the SCF^{Skp2} ubiquitin ligase after p27 is phosphorylated on T187. However, the *in vivo* role of this Skp2 function has remained unclear because of divergent findings from Skp2-null mice (in which all Skp2 functions are absent) and p27T187A knock-in mice (in which only Skp2's ability to mediate ubiquitination of T187-phosphorylated p27 is absent). Skp2-null mice showed p27 protein accumulation in certain tissues and smaller body sizes[14], but p27T187A knock-in mice neither showed p27 protein accumulation nor phenocopied Skp2-null mice[15]. Thus, *in vivo*, Skp2's ability to mediate ubiquitination of T187-phosphorylated p27 does not figure importantly in its ability to regulate p27. Our previous finding that pRb inhibits Skp2-mediated p27 ubiquitination by interfering with Skp2 binding to T187-phosphorylated p27 (ref. 7) suggested that this Skp2 function may be deregulated and contribute to p27 protein reduction and tumorigenesis following *Rb1* loss. To evaluate this prediction, we generated $POMC\text{-}Cre,Rb1^{lox/lox}p27^{T187A/T187A}$ and the control $Rb1^{lox/lox}p27^{T187A/T187A}$ mice and examined their pituitary intermediate lobes at 4, 7 and 11 weeks of age.

The intermediate lobes of $Rb1^{lox/lox}$ $p27^{T187A/T187A}$ mice appeared normal (**Fig. 4a,i**), consistent with the general lack of abnormality in $p27^{T187A/T187A}$ mice. Following *POMC-Cre*–mediated *Rb1* deletion, intermediate lobes of $POMC\text{-}Cre,Rb1^{lox/lox}p27^{T187A/T187A}$ mice at 4 weeks of age did not show the hyperplastic thickening observed in $POMC\text{-}Cre,Rb1^{lox/lox}$ mice (**Fig. 3b, vi**), but instead had regional thinning (**Fig. 4a, ii**). The thinning of the intermediate lobe became more widespread by 7 weeks of age (**Fig. 4a, iii**), and by the age of 11 weeks the entire intermediate lobes were only two to three cell layers thick (**Fig. 4a, iv**). The nature of the T187A knock-in mutation (blocking T187 phosphorylation–dependent ubiquitination of p27 by SCF^{Skp2}) predicted that the tumor-blocking effects observed in $p27^{T187A/T187A}$ homozygous mice should also occur in $p27^{T187A/+}$ heterozygous mice, though potentially to a smaller extent. Results shown in **Figure 4b** confirm this prediction.

Similar to the effects of *Skp2* knockout in *Rb1*-deficient melanotrophs, p27T187A knock-in did not reduce the deregulated expression of PCNA and proliferation (**Fig. 4a, v–vii,ix–xi,** and **c**), but it increased apoptosis (**Fig. 4a, xii–xiv,** and **b**). These effects were also observed in the presence of one allele of p27T187A (**Fig. 4b–d** and data not shown). Finally, the reduced p27 expression in melanotrophs in 4-week-old $POMC\text{-}Cre,Rb1^{lox/lox}$ mice (**Fig. 3b, x**) occurred neither in melanotrophs in either 4- or 7-week-old $POMC\text{-}Cre,Rb1^{lox/lox}p27^{T187A/T187A}$ mice (**Fig. 4a, xv–xvii**) nor in 7-week-old $POMC\text{-}Cre,Rb1^{lox/lox}p27^{T187A/+}$ mice (data not shown). Together these results suggest that the T187 phosphorylation–dependent ubiquitination of p27 by the SCF^{Skp2} ubiquitin ligase underlies Skp2's essential role in pituitary tumorigenesis following *Rb1* loss, and that the apoptotic ablation of melanotrophs in $POMC\text{-}Cre;Rb1^{lox/lox}Skp2^{-/-}$ mice could be explained by a proapoptotic effect of p27 in these cells[16].

Notably, p27T187A knock-in is not equivalent to Skp2 knockout, because the intermediate lobes of $POMC\text{-}Cre,Rb1^{lox/lox}Skp2^{-/-}$ mice thinned to a greater degree and with faster kinetics than those in $POMC\text{-}Cre,Rb1^{lox/lox}p27^{T187A/T187A}$ mice (for example, compare **Fig. 2b, iii,vii** with **Fig. 4a, iii,iv**). Skp2 has a growing list of potential substrates in addition to p27 and can support cancer cell survival by protecting cyclin A from inhibition by p27 and p21 (ref. 17) and by blocking p53 activation by p300 (ref. 18). Further studies will be required to determine the roles of these additional mechanisms.

We next investigated whether the survival function of Skp2 revealed with mouse models was applicable to human tumors that develop as a result of *Rb1* mutations. Because retinoblastoma is the main tumor that is associated with *Rb1* deficiency in humans, we examined the effect of Skp2 knockdown in retinoblastoma cells. We found that

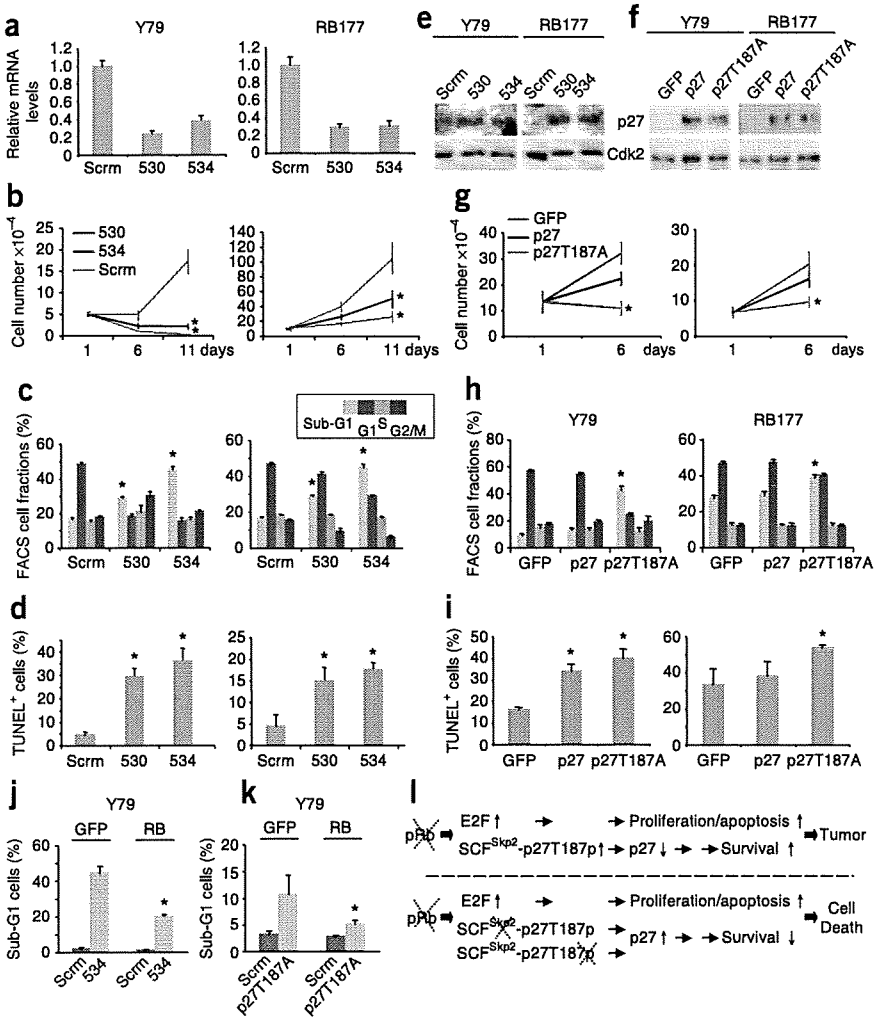

Figure 5 Effects of Skp2 knockdown and stabilized p27 expression on established Y79 cells and early passage RB177 retinoblastoma cells. (**a–e**) Y79 and RB177 cells infected with lentiviruses expressing short hairpin RNAs (shRNAs) targeting Skp2. Two independent Skp2 shRNAs and a scrambled shRNA control (Scrm) were used as indicated. After drug selection, infected cells were evaluated for Skp2 mRNA by quantitative reverse transcriptase PCR (**a**), cell proliferation by counting live cells (**b**), cell cycle profile by FACS (**c**), apoptosis by TUNEL staining (**d**) and p27 expression by protein immunoblotting, with Cdk2 as a loading control (**e**). (**f–i**) Y79 and RB177 cells infected with BE-GFP lentiviral vector encoding *p27* or *p27T187A*. Infected cells were evaluated for p27 expression (**f**), cell proliferation (**g**), cell cycle profile (**h**) and TUNEL staining (**i**). (**j,k**) Y79 cells transduced with BE-GFP vector or BE-GFP-RB, followed 2 d later by transduction with *Skp2* shRNA or scrambled shRNA control (**j**) or with BE-GFP or BE-GFP-p27T187A (**k**), and evaluated cells with sub-G1 DNA content. Averages with s.d. are shown. Asterisks indicate $P < 0.05$ relative to applicable controls. (**l**) A new model of tumorigenesis after *Rb1* loss. Two consecutive arrows suggest the presence of multiple steps between them.

knockdown of Skp2 (**Fig. 5a**) significantly inhibited retinoblastoma cell proliferation (**Fig. 5b**). Skp2 knockdown induced apoptosis, as measured by sub-G1 DNA content and TUNEL staining, but did not diminish S-phase population, as measured by FACS (**Fig. 5c,d**). The apoptotic effects of Skp2 knockdown were evident both in the established Y79 cell line and in early-passage RB177 cells.

As expected, Skp2 knockdown induced accumulation of p27 in these human retinoblastoma cells (**Fig. 5e**). Moreover, ectopic expression of p27 was able to inhibit proliferation and induce apoptosis (**Fig. 5f–i**) similar to the effects of Skp2 knockdown. Notably, the mutant p27T187A was considerably more potent in inhibiting proliferation and inducing apoptosis, consistent with our findings from p27T187A knock-in mice. Restoration of pRb function largely prevented apoptosis induced either by Skp2 knockdown or by ectopic p27 expression (**Fig. 5j,k**), even though the modest pRb concentrations slowed but did not entirely block cell proliferation (data not shown), suggesting that lack of pRb rendered the retinoblastoma cells dependent on Skp2 and sensitive to aberrantly expressed p27.

We recently showed that MDM2 has essential roles in proliferation and survival of retinoblastoma cells and that knockdown of p14Arf diminished the requirement for MDM2 (ref. 19). In similar experiments we found that knockdown of p14Arf did not mitigate the effects of Skp2 knockdown, suggesting that p14Arf is not a critical target of Skp2 in these cells (**Supplementary Fig. 4**).

Before the current study, inactivation of previously studied pRb targets delayed tumorigenesis in $Rb1^{+/-}$ mice accompanied by reduced tumor cell proliferation[1–6]. In contrast, our study reveals that inactivation of Skp2 did not reduce deregulated proliferation of $Rb1^{-/-}$ cells but induced apoptosis, which completely prevented tumorigenesis. Our findings add a survival arm to the pRb-E2F model of pRb function, in which pRb loss not only deregulates E2F to result in aberrant proliferation and apoptosis through various E2F target genes but also deregulates the SCF^{Skp2}-p27T187p p27 ubiquitination mechanism to downregulate p27 to provide survival support for the aberrantly proliferating pRb-deficient cells (**Fig. 5l**). When this mechanism is disrupted, either by inactivation of Skp2 or by blocking of p27 T187 phosphorylation, the outcome of pRb loss becomes cell death, revealing that *Rb1* and *Skp2* mutations are synthetically lethal to susceptible cells. The above model predicts that Skp2 is a potentially effective drug target to prevent and treat pRb-deficient tumors. Because our data imply that the p27T187 phosphorylation–dependent function of Skp2 is required for tumorigenesis following pRb loss, yet is not needed for normal development[15], therapeutic targeting of Skp2 can focus on the p27T187-dependent function of Skp2 or p27T187 phosphorylation.

METHODS

Methods and any associated references are available in the online version of the paper at http://www.nature.com/naturegenetics/.

Note: Supplementary information is available on the Nature Genetics website.

ACKNOWLEDGMENTS

We thank J. Cui for expert technical assistance, R. Mahmood for help with tissue preparation and histological analysis, D. Abramson and S. Jhanwar for support of retinoblastoma cell analysis, A. Koff for comments on the manuscript and A. Burns and W. Zhang for encouragement. We are grateful to T. Jacks for providing $Rb1^{+/-}$

mice (from L. Yamasaki and A. Iavarone) and $Rb1^{lox/lox}$ mice, B. Lowell and S. Chua for *POMC-Cre* mice, J. Roberts for p27T187A knock-in mice and F. Costantini for Rosa26YFP mice (from J. Pollard). This work was supported by grants from the National Institute of Diabetes and Digestive and Kidney Diseases and National Cancer Institute of the US National Institutes of Health to L.Z. Albert Einstein Comprehensive Cancer Research Center and Liver Research Center provided core facility support. F.B. was supported by the Training Program in Cellular and Molecular Biology and Genetics (T32 GM007491) at the Albert Einstein College of Medicine. L.Z. is a recipient of the Irma T. Hirschl Career Scientist Award.

AUTHOR CONTRIBUTIONS

H.W., P.J., F.B., D.S. and L.Z. designed and performed experiments with mice mutant for *Rb1*, *Skp2*, *p27* or targeted deletion of *Rb1*. J.L. and R.S.S. performed pathology studies. D.C. and X.X. designed and performed analyses of retinoblastoma cells; H.W. performed protein blot experiments. K.N. and K.I.N. provided $Skp2^{+/-}$ mice. H.W., J.L., D.C. and L.Z. wrote the paper.

Published online at http://www.nature.com/naturegenetics/.
Reprints and permissions information is available online at http://npg.nature.com/reprintsandpermissions/.

1. Yamasaki, L. *et al.* Loss of E2F–1 reduces tumorigenesis and extends the lifespan of $Rb1^{+/-}$ mice. *Nat. Genet.* **18**, 360–364 (1998).
2. Ziebold, U., Lee, E.Y., Bronson, R.T. & Lees, J.A. E2F3 loss has opposing effects on different pRB-deficient tumors, resulting in suppression of pituitary tumors but metastasis of medullary thyroid carcinomas. *Mol. Cell. Biol.* **23**, 6542–6552 (2003).
3. Lee, E.Y. *et al.* E2F4 loss suppresses tumorigenesis in Rb mutant mice. *Cancer Cell* **2**, 463–472 (2002).
4. Lasorella, A., Rothschild, G., Yokota, Y., Russell, R.G. & Iavarone, A. Id2 mediates tumor initiation, proliferation, and angiogenesis in Rb mutant mice. *Mol. Cell. Biol.* **25**, 3563–3574 (2005).
5. Takahashi, C. *et al.* Nras loss induces metastatic conversion of Rb1-deficient neuroendocrine thyroid tumor. *Nat. Genet.* **38**, 118–123 (2006).
6. Takahashi, C., Contreras, B., Bronson, R.T., Loda, M. & Ewen, M.E. Genetic interaction between Rb and K-ras in the control of differentiation and tumor suppression. *Mol. Cell. Biol.* **24**, 10406–10415 (2004).
7. Ji, P. *et al.* An Rb-Skp2-p27 pathway mediates acute cell cycle inhibition by Rb and is retained in a partial-penetrance Rb mutant. *Mol. Cell* **16**, 47–58 (2004).
8. Binne, U.K. *et al.* Retinoblastoma protein and anaphase-promoting complex physically interact and functionally cooperate during cell-cycle exit. *Nat. Cell Biol.* **9**, 225–232 (2007).
9. Frescas, D. & Pagano, M. Deregulated proteolysis by the F-box proteins SKP2 and beta-TrCP: tipping the scales of cancer. *Nat. Rev. Cancer* **8**, 438–449 (2008).
10. Zhang, L. & Wang, C. F-box protein Skp2: a novel transcriptional target of E2F. *Oncogene* **25**, 2615–2627 (2005).
11. Yung, Y., Walker, J.L., Roberts, J.M. & Assoian, R.K.A. Skp2 autoinduction loop and restriction point control. *J. Cell Biol.* **178**, 741–747 (2007).
12. Jacks, T. *et al.* Effects of an Rb mutation in the mouse. *Nature* **359**, 295–300 (1992).
13. Vooijs, M., van der Valk, M., te Riele, H. & Berns, A. Flp-mediated tissue-specific inactivation of the retinoblastoma tumor suppressor gene in the mouse. *Oncogene* **17**, 1–12 (1998).
14. Nakayama, K. *et al.* Targeted disruption of Skp2 results in accumulation of cyclin E and p27(Kip1), polyploidy and centrosome overduplication. *EMBO J.* **19**, 2069–2081 (2000).
15. Malek, N.P. *et al.* A mouse knock-in model exposes sequential proteolytic pathways that regulate p27Kip1 in G1 and S phase. *Nature* **413**, 323–327 (2001).
16. Carneiro, C. *et al.* p27 deficiency desensitizes $Rb^{-/-}$ cells to signals that trigger apoptosis during pituitary tumor development. *Oncogene* **22**, 361–369 (2003).
17. Ji, P., Sun, D., Wang, H., Bauzon, F. & Zhu, L. Disrupting Skp2-cyclin A interaction with a blocking peptide induces selective cancer cell killing. *Mol. Cancer Ther.* **6**, 684–691 (2007).
18. Kitagawa, M., Lee, S.H. & McCormick, F. Skp2 suppresses p53-dependent apoptosis by inhibiting p300. *Mol. Cell* **29**, 217–231 (2008).
19. Xu, X.L. *et al.* Retinoblastoma has properties of a cone precursor tumor and depends upon cone-specific MDM2 signaling. *Cell* **137**, 1018–1031 (2009).

ONLINE METHODS

Mice. $Rb1^{+/-}$ mice and $Skp2^{+/-}$ mice have been described elsewhere[12,14]. Mouse strain background is as follows. $Skp2^{+/-}$ mice on mixed C57BL/6J×129Sv strain background were backcrossed to C57BL/6J strain mice four times, and $Rb1^{+/-}$ mice on mixed C57BL/6J×129Sv strain background were backcrossed to C57BL/6J mice once. $Rb1^{+/-}Skp2^{+/-}$ mice were then generated from these mice and were used to generate littermate $Rb1^{+/-}Skp2^{+/+}$ and $Rb1^{+/-}Skp2^{-/-}$ mice. Our $Rb1^{+/-}$ mice may therefore show a slower tumor development kinetics than $Rb1^{+/-}$ mice with equal contributions from C57BL/6J and 129Sv strain background[20]. *Rb1*-heterozygous mice were genotyped according to a published protocol[12]. *POMC-Cre* transgenic mice were genotyped as described[21]. Primers for genotyping $Skp2^{+/-}$ mice, $Rb1^{lox/lox}$ mice[22], *Rosa26R*(YFP) mice[23] and p27T187A knock-in mice[15] are listed in **Supplementary Table 1**.

The animals studied for ENU mutagenesis were C57BL/6J×129Sv hybrid strain littermate mice from Skp2 heterozygous crosses. $Skp2^{+/+}$ and $Skp2^{-/-}$ mice were injected intraperitoneallywith ENU (0.5 mmol per g body weight) at P15 ± 2 d as described[24]. Mice were killed at the first sign of morbidity, which included abdominal swelling, hunched posture and rapid breathing. Complete necropsies of all internal organs were performed including size measurement of tumors.

All mouse study protocols were approved by the Albert Einstein College of Medicine Animal Institute.

Protein blot and reverse transcriptase–PCR analyses. Normal pituitaries, fractions of gross pituitary tumors and fractions of ENU-induced tumors were snap-frozen in ethanol–dry ice and stored in −80 °C. For protein blot, frozen tissues were homogenized with Dounce glass homogenizer in tissue lysis buffer (50 mM HEPES, pH 7.2, 150 mM NaCl, 1 mM EDTA, 0.1% Tween-20, 1 mM dithiothreitol and standard protease inhibitors). Tissue debris was removed by centrifugation for 10 min at 14,000 r.p.m. in an Eppendorf Centrifuge 5415C (F-45-18-11 rotor) at 4 °C. Protein concentrations of the extracts were determined by Bio-Rad protein assay kit, and equal amounts of protein samples were loaded on 10% SDS gels and blotted onto polyvinylidene fluoride membrane. Antibodies to Skp2 (H435), p27 (C-19), cyclin A (C-19), cyclin E (M-20) and Cdk2 (C-19) were from Santa Cruz Biotechnology.

For quantitative PCR (Q-PCR), tissue RNA was extracted by Trizol reagent (Invitrogen). Total RNA was treated with RQ1 DNase (Promega) at 37 °C for 30 min, and RQ1 was denatured at 65 °C for 20 min. T7 oligonucleotides and SuperScript II (Invitrogen) were used for the synthesis of the first-strand cDNA at 42 °C for 60 min. The PCR primers for mSkp2 and mGAPDH are listed in **Supplementary Table 1**. SYBR Green PCR Master Mix (4309155; ABI) and the standard program of ABI Prism 7000 were used for Q-PCR amplification.

Immunohistochemistry staining and frozen sectioning for fluorescence detection. Paraffin sections were stained with Histomouse-plus kit (Zymed) with antibodies to PCNA (PC10) and p27 (C-19) from Santa Cruz Biotechnology, and to BrdU (Ab-2) from Calbiochem, and Ki67 as primary antibody (1 μg/ml). TUNEL staining was performed with the reagents and instructions of Apoptosis Detection Kit (S7101) from Chemicon.

Pituitaries were fixed in 4% paraformaldehyde, 10% glucose in PBS for 30 min and embedded in Tissue Freezing Medium (H-TFM; Triangle Biomedical Sciences) on dry ice for frozen sectioning. After fluorescence photography, slides were counterstained by hematoxylin.

Lentivirus infection and analysis of human retinoblastoma cells. Y79 cells were purchased from the American Type Culture Collection, and RB177 cells were derived from a human retinoblastoma and passaged for approximately 2 months, with no evidence of a crisis phase, before the knockdown analyses[19]. Skp2 shRNAs were delivered by pLKO constructs TRCN0000007530 and TRCN0000007534 (Open Biosystems) and were compared to a pLKO encoding a nonsilencing control shRNA (Addgene). RB177 cells with constitutive $CDKN2A^{ARF}$-null and pLKO-transduced controls were as described[19]. pRb, p27 and p27T187A were delivered using the bidirectional BE-GFP vector[25]. BE-GFP-p27+3′ and BE-GFP-p27T187A+3′ were produced by inserting a XmaI-XbaI fragment of pCS+p27 and pCS+p27(T187A)[26] extending from the p27 coding region to the 3′ UTR between the corresponding XmaI site and a vector XbaI site of BE-GFP-p27 (ref. 25). BE-GFP-Rb was as described[25]. Cells were cultured, infected and analyzed as described[19].

Statistical analysis. In the survival analysis, difference in Kaplan-Meier survival curves was analyzed by log-rank test (JMP Software). Differences in gross tumor incidence and incidence of microscopic lesions in macroscopically normal pituitary and thyroid glands were analyzed by Fisher's exact test (MedCalc Software). Differences in TUNEL-labeling indices between $Rb1^{lox/lox}$;*POMC-Cre*;$Skp2^{+/+}$ and $Rb1^{lox/lox}$;*POMC-Cre*;$Skp2^{-/-}$ intermediate lobes and between $Rb1^{lox/lox}$;*POMC-Cre*;$p27^{+/+}$ and $Rb1^{lox/lox}$;*POMC-Cre*;$p27^{T187A/T187A}$ intermediate lobes were analyzed by Student's *t*-test (MedCalc Software).

20. Leung, S.W. *et al.* A dynamic switch in $Rb^{+/-}$ mediated neuroendocrine tumorigenesis. *Oncogene* **23**, 3296–3307 (2004).
21. Balthasar, N. *et al.* Leptin receptor signaling in POMC neurons is required for normal body weight homeostasis. *Neuron* **42**, 983–891 (2004).
22. Sage, J., Miller, A.L., Perez-Mancera, P.A., Wysocki, J.M. & Jacks, T. Acute mutation of retinoblastoma gene function is sufficient for cell cycle re-entry. *Nature* **424**, 223–228 (2003).
23. Srinivas, S. *et al.* Cre reporter strains produced by targeted insertion of *EYFP* and *ECFP* into the *ROSA26* locus. *BMC Dev. Biol.* **1**, 4 (2001).
24. Timmerbeul, I. *et al.* Testing the importance of p27 degradation by the SCFskp2 pathway in murine models of lung and colon cancer. *Proc. Natl. Acad. Sci. USA* **103**, 14009–14014 (2006).
25. Cobrinik, D., Francis, R.O., Abramson, D.H. & Lee, T.C. Rb induces a proliferative arrest and curtails Brn-2 expression in retinoblastoma cells. *Mol. Cancer* **5**, 72 (2006).
26. Sheaff, R.J., Groudine, M., Gordon, M., Roberts, J.M. & Clurman, B.E. Cyclin E-CDK2 is a regulator of p27Kip1. *Genes Dev.* **11**, 1464–1478 (1997).

THE JOURNAL OF BIOLOGICAL CHEMISTRY VOL. 285, NO. 7, pp. 4837–4846, February 12, 2010

Phospholipase C-related but Catalytically Inactive Protein Is Required for Insulin-induced Cell Surface Expression of γ-Aminobutyric Acid Type A Receptors*

Received for publication, September 24, 2009, and in revised form, December 1, 2009 Published, JBC Papers in Press, December 7, 2009, DOI 10.1074/jbc.M109.070045

Makoto Fujii[‡1], Takashi Kanematsu[‡2], Hitoshi Ishibashi[§], Kiyoko Fukami[¶], Tadaomi Takenawa[‖], Keiichi I. Nakayama[**], Stephen J. Moss[‡‡], Junichi Nabekura[§], and Masato Hirata[‡3]

From the [‡]Laboratory of Molecular and Cellular Biochemistry, Faculty of Dental Science, and Station for Collaborative Research, Kyushu University, Fukuoka 812-8582, Japan, the [§]Department of Developmental Physiology, National Institute for Physiological Sciences, Okazaki 444-8585, Japan, the [¶]Laboratory of Genome and Biosignal, Tokyo University of Pharmacy and Life Science, Tokyo 192-0392, Japan, the [‖]Department of Lipid Biochemistry, Kobe University Graduate School of Medicine, Kobe 650-0017, Japan, the [**]Department of Molecular and Cellular Biology, Medical Institute of Bioregulation, Kyushu University, Fukuoka 812-8582, Japan, and the [‡‡]Department of Neuroscience, Tufts University School of Medicine, Boston, Massachusetts 02111

The γ-aminobutyric acid type A ($GABA_A$) receptors play a pivotal role in fast synaptic inhibition in the central nervous system. One of the key factors for determining synaptic strength is the number of receptors on the postsynaptic membrane, which is maintained by the balance between cell surface insertion and endocytosis of the receptors. In this study, we investigated whether phospholipase C-related but catalytically inactive protein (PRIP) is involved in insulin-induced $GABA_A$ receptor insertion. Insulin potentiated the GABA-induced Cl^- current (I_{GABA}) by about 30% in wild-type neurons, but not in PRIP1 and PRIP2 double-knock-out (DKO) neurons, suggesting that PRIP is involved in insulin-induced potentiation. The phosphorylation level of the $GABA_A$ receptor β-subunit was increased by about 30% in the wild-type neurons but not in the mutant neurons, which were similar to the changes observed in I_{GABA}. We also revealed that PRIP recruited active Akt to the $GABA_A$ receptors by forming a ternary complex under insulin stimulation. The disruption of the binding between PRIP and the $GABA_A$ receptor β-subunit by PRIP interference peptide attenuated the insulin potentiation of I_{GABA}. Taken together, these results suggest that PRIP is involved in insulin-induced $GABA_A$ receptor insertion by recruiting active Akt to the receptor complex.

The γ-aminobutyric acid (GABA)[4] type A ($GABA_A$) receptors are GABA-gated chloride channels that mediate the majority of fast synaptic inhibition in the central nervous system (1–5). The perturbation of GABA-$GABA_A$ receptors-mediated neurotransmission causes several central nervous system disorders including motor coordination, anxiety, insomnia, schizophrenia, and epilepsy. Additionally, $GABA_A$ receptors are important therapeutic drug targets for sedative, anxiolytic, anticonvulsant, and hypnotic agents (1–5). Therefore, it is important to uncover how synaptic strength is regulated in GABAergic transmission. The $GABA_A$ receptors are heteropentamers composed of a combination of 18 $GABA_A$ receptor subunits, which are divided into seven subunit classes (α1–6, β1–3, γ1–3, δ, ε1–3, θ, and π) based on their sequence homology (1–5). Each receptor subunit has a similar structure with a large N-terminal extracellular region, which is the binding site for GABA and psychoactive drugs such as benzodiazepines, followed by four hydrophobic transmembrane domains (TM1–4) with a large intracellular loop region between TM3 and 4. This intracellular loop region is a target for protein-protein interactions, phosphorylation, ubiquitination, and palmitoylation, which control receptor trafficking, stability, and clustering on the synaptic membrane (1–5). Regulation of the number of receptors on the postsynaptic membrane is one of the key factors for determining synaptic strength, which is maintained by a balance between the insertion and endocytosis of receptors to/from the cell surface. Recently, it was reported that the dephosphorylation of the $GABA_A$ receptor β- or γ2-subunit triggers endocytosis by facilitating the binding to the μ2-subunit of adaptor protein 2 (AP2) complex, a critical component of clathrin-dependent endocytosis (6–9). On the other hand, it was reported that insulin stimulates $GABA_A$ receptor insertion into the cell surface membrane via Akt-mediated phosphorylation of the $GABA_A$ receptor β-subunit (10–14).

We previously identified a new inositol 1,4,5-trisphosphate-binding protein from rat brain lysate by affinity column chromatography (15). Our subsequent studies on the characterization of the protein revealed that 1) it has a domain organization

* This work was supported by grants from the Ministry of Education, Culture, Sports, Science, and Technology of Japan (to M. F., T. K., and M. H.), the Cooperative Study Program of the National Institute for Physiological Sciences (to T. K., J. N., and M. H.), the Japan Diabetes Foundation (to T. K.), and the Pharmacological Research Foundation, Tokyo (to T. K.).

[1] Research Fellow supported by the Japan Society for the Promotion of Science.

[2] Present address: Dept. of Dental Pharmacology, Graduate School of Biomedical Sciences, Hiroshima University, Hiroshima 734-8553, Japan.

[3] To whom correspondence should be addressed. Tel.: 81-92-642-6317; Fax: 81-92-642-6322; E-mail: hirata1@dent.kyushu-u.ac.jp.

[4] The abbreviations used are: GABA, γ-aminobutyric acid; AP2, adaptor protein 2; BDNF, brain-derived neurotrophic factor; DIV, days *in vitro*; DKO, PRIP1 and PRIP2 double knockout; $GABA_A$ receptor, γ-aminobutyric acid type A receptor; GABARAP, $GABA_A$ receptor-associated protein; GST, glutathione *S*-transferase; I_{GABA}, GABA-induced Cl^- current; PP, protein phosphatase; PRIP, phospholipase C-related but catalytically inactive protein; WT, wild-type; NSF, *N*-ethylmaleimide-sensitive factor; PI, phosphatidylinositol.

similar to δ-type phospholipase C (PLC) but has no PLC activity, which is the reason for its name, PRIP (PLC-related but catalytically inactive protein) (16, 17). 2) PRIP has two isoforms, PRIP1 and 2, which are expressed mainly in the brain and ubiquitous organs, respectively (18–20). 3) PRIP knock-out mice are less sensitive to benzodiazepine-type drugs, such as diazepam, suggesting that the cell surface expression of γ-subunit-containing GABA$_A$ receptors is diminished in these mutant mice (21, 22). 4) PRIP facilitates GABA$_A$ receptor-associated protein (GABARAP) mediated cell surface expression of γ2-subunit-containing GABA$_A$ receptors by acting as a bridging molecule between GABARAP and receptors (22–24). 5) PRIP regulates the phosphorylation level of the GABA$_A$ receptor β-subunit by binding to protein phosphatases (25–27). 6) PRIP is involved in clathrin-dependent constitutive endocytosis of GABA$_A$ receptors (28). We also have reported that PRIP modulates brain-derived neurotrophic factor (BDNF)-induced GABA$_A$ receptor endocytosis through the regulation of the receptor phosphorylation level (29). These results suggest that PRIP regulates GABA$_A$ receptor function through receptor trafficking, phosphorylation, and endocytosis (30, 31).

In this study, we investigated whether PRIP is involved in insulin-induced GABA$_A$ receptor insertion. Insulin potentiated the GABA-induced Cl^- current (I_{GABA}) by about 30% in wild-type (WT) hippocampal neurons but not in neurons derived from PRIP1 and PRIP2 double knock-out (DKO) mice. The phosphorylation level of the β-subunit was increased by about 30% in the WT neurons but not in the DKO neurons, which was similar to the changes observed in I_{GABA}. Using an immunoprecipitation assay and a glutathione *S*-transferase (GST) pull-down assay using brain lysate together with a HEK293 reconstitution system we revealed that PRIP recruited active Akt to GABA$_A$ receptors. The disruption of the binding between PRIP and the β-subunit by PRIP interference peptide attenuated the insulin-potentiated I_{GABA}. Interestingly, pretreatment with brefeldin A (BFA), an inhibitor of anterograde trafficking from the ER to the Golgi (32, 33) decreased I_{GABA} under insulin treatment. Collectively, these results suggest that PRIP plays an important role in insulin-induced GABA$_A$ receptor insertion by recruiting active Akt to the receptor complex.

EXPERIMENTAL PROCEDURES

Chemicals, Plasmids, and Animals—Insulin and okadaic acid were obtained from Wako. Wortmannin, BFA, and crosstide were purchased from Sigma. The PRIP1-(553–565) peptide and its scrambled peptide were described previously (29). Anti-PRIP1 and anti-PRIP2 polyclonal antibodies were described previously (20, 21). Anti-Akt polyclonal antibody, antiphospho-Akt (Thr-308 or Ser-473) polyclonal antibodies, and anti-insulin receptor β-subunit monoclonal antibody (clone 4B8) were purchased from Cell Signaling. Anti-GABA$_A$ receptor α1-subunit and anti-GABA$_A$ receptor γ2-subunit polyclonal antibodies were obtained from Alpha Diagnostic International. Anti-GABA$_A$ receptor β2/3-subunit monoclonal antibody (clone 62–3G1) and anti-*N*-ethylmaleimide-sensitive factor (NSF) polyclonal antibody were from Upstate. Anti-GST polyclonal antibody was purchased from Santa Cruz Biotechnology. Horseradish peroxidase-conjugated anti-rabbit and anti-mouse IgG were obtained from GE Healthcare. [^{32}P]Orthophosphate (5.55 GBq/ml) and [γ-^{32}P]ATP (185 MBq/ml, specific activity: 111 TBq/mmol) were purchased from PerkinElmer. Construction of the mammalian expression vectors for the Myc- and FLAG-tagged GABA$_A$ receptor subunit (α1, β2, and γ2S) was described previously (34). Briefly, the Myc or FLAG tag was introduced between amino acids 4 and 5 of the mature form of each receptor subunit. For the mammalian GST fusion protein expression vector pcDNA3.1(-)/GST1, GST was amplified using primers M-81, 5′-AAA AAG CTA GCC ACC ATG TCC CCT ATA CTA GG-3′ (underlining denotes the NheI site) and M-82, 5′-AAA AAC TCG AGA TCG ATA CCG TCG ACC TCG A-3′ (underlining denotes the XhoI site) and pGST4 as a template. The PCR products were digested using NheI/XhoI and cloned into the same sites of pcDNA3.1(-). The rat PRIP1 (rPRIP1) was amplified using primers M-85, 5′-AAA AAC TCG AGC ATG GCT GAG GGC GCG GCT A-3′ (underlining denotes the XhoI site) and M-86, 5′-AAA AAA AGC TTT CAC AAC TTC CCG TTC TCT TC-3′ (underlining denotes the HindIII site) and pcMT31 (16) as a template. The PCR products were digested using XhoI/HindIII and cloned into the same sites of pcDNA3.1(-)/GST1 to produce pcDNA3.1(-)/GST1-rPRIP1. The PRIP1 expression plasmid pSG5/rPRIP1 was described previously (16). The mammalian expression vector for Akt pECE/Akt was kindly provided by Dr. U. Kikkawa (Kobe University, Japan) (35). The generation of the DKO mice was described previously (22, 29). The handling of the mice and all procedures were approved by the Animal Care Committee of Kyushu University, according to the guidelines of the Japanese Council on Animal Care.

Electrophysiology—Electrophysiological measurements were performed in acutely isolated hippocampal CA1 pyramidal neurons using the conventional whole cell patch-clamp technique. The acutely dissociated neurons were prepared from postnatal day 10–14 WT or DKO mice, as described previously (36). All recordings were performed under voltage clamp conditions at a holding potential of −50 mV and a patch-clamp amplifier (EPC-7plus, HEKA Instruments Inc). All experiments were performed at a room temperature of 22–25 °C. The ionic composition of patch pipette solution containing 80 mM KCl, 70 mM potassium methanesulfonate, 4 mM ATP-Mg, 2 mM EGTA, 1 mM $MgCl_2$, 10 mM HEPES, and adjusted pH to 7.2 with Tris-base. Extracellular solution containing 150 mM NaCl, 2.5 mM KCl, 2 mM $CaCl_2$, 1 mM $MgCl_2$, 10 mM HEPES, and 10 mM glucose. The pH was adjusted to 7.4 with Tris-base. Reagents dissolved in extracellular solution were applied by using the Y-tube perfusion system, which allows rapid exchange of the solution surrounding a cell (37, 38). All data are expressed as the means ± S.D.

Cell Culture and Transfection—HEK293 cells were grown in Dulbecco's modified Eagle's medium (DMEM) containing 10% fetal bovine serum supplemented with 100 units/ml penicillin and 0.1 mg/ml streptomycin. The cells were maintained at 37 °C in a humidified 5% CO_2 incubator. Plasmid transfection was performed using the calcium phosphate method as described elsewhere (39) or Lipofectamine 2000 (Invitrogen) according to the manufacturer's protocol. Briefly, 1.5 μg of each GABA$_A$ receptor subunit (α1, β2, and γ2S) with or without 2.5

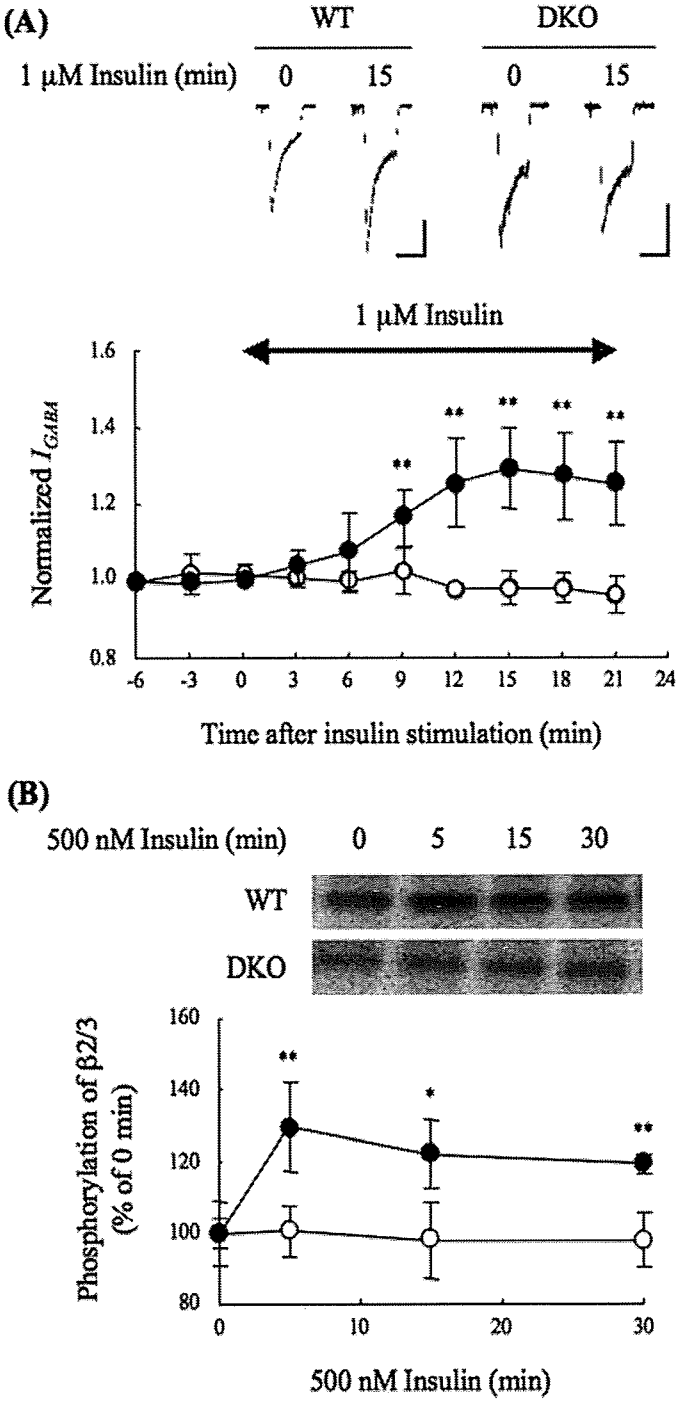

FIGURE 1. **Electrophysiological analysis of I_{GABA} in insulin-stimulated hippocampal CA1 neurons and phosphorylation of the GABA$_A$ receptor β2/3-subunit.** *A*, effect of insulin on I_{GABA}. Electrophysiological experiments were performed using acutely prepared hippocampal CA1 neurons from WT (*closed circles*, $n = 5$) or DKO (*open circles*, $n = 5$) mice. GABA (3 μM) was applied for 15 s (3-min interval), and whole cell currents were recorded. Insulin (1 μM) was applied for the time period indicated by the *double-headed arrow* in graph. *Upper panel* shows representative GABA-induced current traces at 0 min or 15 min after insulin stimulation of WT or DKO neurons. *Vertical* and *horizontal scales* show 200 pA and 15 s, respectively. The graph shows the amplitude of I_{GABA} normalized to that seen without insulin. All data are represented as means ± S.D. Significance was determined using the Student's *t* test (**, $p < 0.01$, compared with the results from DKO). *B*, phosphorylation of the β-subunit in response to insulin stimulation. The cultured cortical neurons (DIV. 14–18) of the WT or DKO mice were metabolically labeled with [^{32}P]orthophosphates for 4 h. The neurons were stimulated with 500 nM insulin for the indicated time, and then the cell lysates were subjected to immunoprecipitation using an anti-GABA$_A$ receptor β2/3-subunit antibody. The immunocomplexes were separated by SDS-PAGE and then subjected to autoradiography. Phosphorylated bands were detected using BAS2500. The autoradiograph represents one of four independent experiments. The other experiments gave similar results. The graph shows quantitative data concerning the phosphorylation of the GABA$_A$ receptor β2/3-subunit of WT (*closed circles*) or DKO (*open circles*) neurons. As mentioned above, ^{32}P incorporation was analyzed, because the phosphospecific antibody currently available recognizes the di-phosphorylated β3-subunit at both Ser-408 and Ser-409 (29, 41), and insulin causes a single phosphorylation at Ser-410 or Ser-409 of β2- or β3-subunit, respectively (11, 12). Data are represented as means ± S.D. ($n = 4$). Significance was determined using the Student's *t* test (*, $p < 0.05$; **, $p < 0.01$, compared with the results from DKO).

μg of pSG5/rPRIP1 and/or pECE/Akt were transfected into 7.5×10^5 cells. For the GST pull-down assay, 1.0 μg of pcDNA3.1(-)/GST1 or pcDNA3.1(-)/GST1-rPRIP1 was transfected with 2.5 μg of pECE/Akt. After 48 h of incubation, the cells were used for each experiment. Cortical neurons were prepared from postnatal day 0 (P0) WT or DKO mice, as described previously (21, 29) and were cultured for 14–18 days *in vitro* (DIV) before the experiments.

Immunoprecipitation, GST Pull-down, and Western Blotting—Cell lysates were prepared from cortical neurons or plasmid-transfected HEK293 cells using ice-cold lysis buffer containing 50 mM Tris-HCl, pH 7.5, 150 mM NaCl, 5 mM EDTA, 1 mM EGTA, 1% Triton X-100, phosphatase inhibitors (50 mM NaF, 10 mM $Na_4P_2O_7$, 20 mM β-glycerophosphate, and 1 mM Na_3VO_4), and protease inhibitors (1 mM phenylmethylsulfonyl fluoride, 100 μM (*p*-amidinophenyl)methanesulfonyl fluoride hydrochloride, 10 μg/ml leupeptin, 10 μg/ml pepstatin A, and 3.4 μg/ml aprotinin). The mouse whole brain lysates of WT or DKO mice were also prepared using the same buffer. In the case of co-precipitation of NSF, 0.5 mM ATP was added to the lysis buffer. The lysates were subjected to immunoprecipitation using the indicated antibodies. For the GST pull-down assay, 20 μl of glutathione-Sepharose™ 4B (GE Healthcare) were added to cell lysates expressing the GST fusion protein. The immunocomplex was washed five times with 1 ml of ice-cold lysis buffer containing phosphatase inhibitors. The lysates and immunocomplexes were subjected to SDS-polyacrylamide gel electrophoresis (PAGE) and then transferred onto polyvinylidene fluoride membrane. Western blotting was performed using the indicated antibodies, and signals were detected using the ECL plus Western blotting detection system (GE Healthcare) and LAS3000 mini (Fuji Film).

^{32}P Labeling of Cultured Neurons—Cultured cortical neurons (DIV 14–18) were incubated with 1 ml of phosphate-free DMEM for 1 h and then labeled with 7.4 MBq/ml of [^{32}P]orthophosphate for 4 h at 37 °C. The neurons were stimulated with 500 nM insulin for the indicated times at 37 °C. The cells were then washed twice with ice-cold phosphate-buffered saline and extracted with 500 μl of ice-cold lysis buffer containing phosphatase inhibitors and protease inhibitors. The cell lysates were subjected to immunoprecipitation using an anti-GABA$_A$ receptor β2/3-subunit monoclonal antibody. The immunocomplexes were washed five times with 1 ml of ice-cold lysis buffer containing phosphatase inhibitors and subjected to SDS-PAGE. Phosphorylated proteins were detected by autoradiography using a Bio-Image analyzer BAS2500 (Fuji Film).

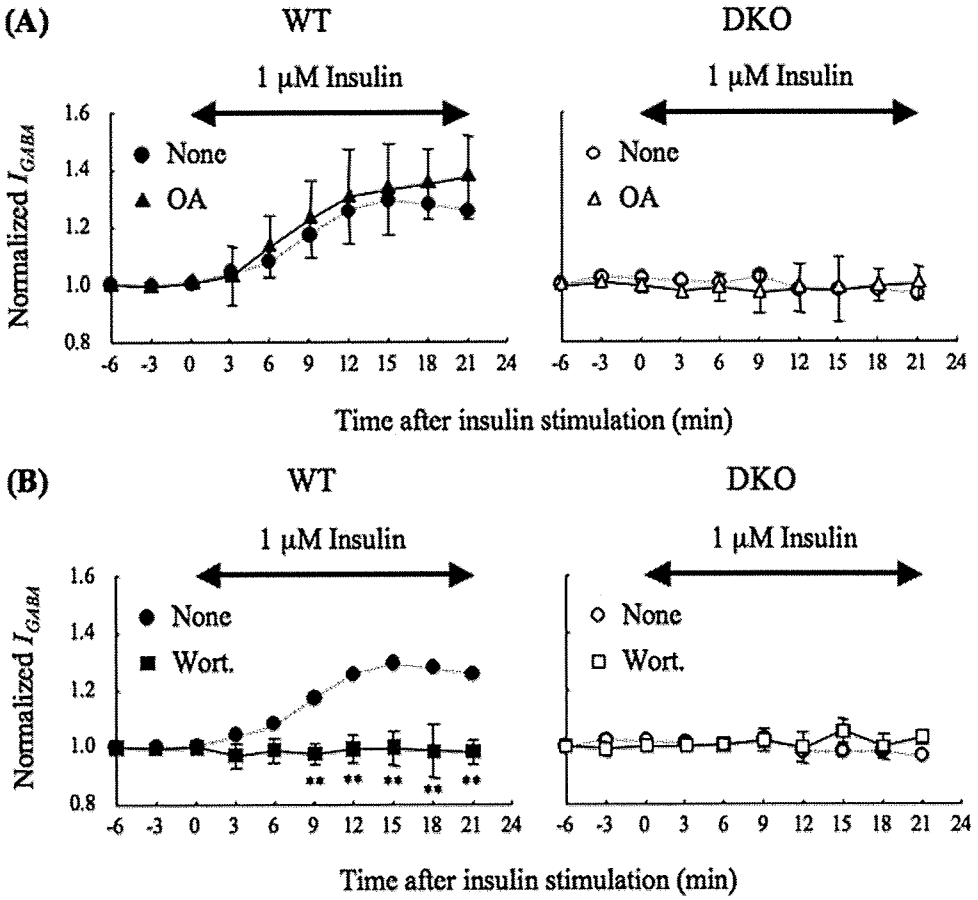

FIGURE 2. **Effect of okadaic acid or wortmannin on the insulin-potentiation of I_{GABA}.** *A*, effect of okadaic acid on the insulin potentiation of I_{GABA}. Neurons from WT (*left panel, closed triangles, n* = 8) or DKO (*right panel, open triangles, n* = 3) mice were pretreated with 10 μM okadaic acid, an inhibitor of the protein phosphatases PP1 and PP2A (42), for 15 min and throughout the experiment. The experiment was performed as shown in Fig. 1*A* except for the okadaic acid treatment. All data are represented as means ± S.D. The I_{GABA} from WT (*left panel, closed circles, dashed line*) or DKO (*right panel, open circles, dashed line*) mice without okadaic acid (none), which were taken from Fig. 1*A*, are also shown as references. *B*, effect of wortmannin on the insulin potentiation of I_{GABA}. Neurons from WT (*left panel, closed squares, n* = 6) or DKO (*right panel, open squares, n* = 3) mice were pretreated with 100 nM of wortmannin, a potent PI 3-kinase inhibitor (45), for 15 min and throughout the experiment. The experiments were performed as shown in Fig. 1*A* except for the wortmannin treatment. All data are represented as means ± S.D. The I_{GABA} from WT (*left panel, closed circles, dashed line*) or DKO (*right panel, open circles, dashed line*) mice without wortmannin (none), which were taken from those shown in Fig. 1*A*, are also shown as references. *Double-headed arrows* indicate the period of insulin stimulation. Significance was determined using the Student's *t* test (**, $p < 0.01$ from the results obtained in the absence of the drug). *none*, no addition; *OA*, okadaic acid; *Wort*, wortmannin.

Akt Kinase Assay—The Akt kinase assay was described previously (40). Briefly, immunocomplexes created using an anti-Akt polyclonal antibody were washed once with ice-cold 1 ml of Akt kinase assay buffer (50 mM Tris-HCl, pH 7.5, 10 mM $MgCl_2$, and 1 mM dithiothreitol) and then resuspended in 30 μl of the same buffer containing 100 μM peptide substrate, crosstide, and 10 μM [γ-^{32}P]ATP (37 kBq/reaction). After incubation for 30 min at 30 °C, the reaction was stopped by adding 10 μl of 300 mM H_3PO_4. The reaction products were spotted onto peptide binding paper (Whatman P81 cation exchange paper) and then washed three times with 75 mM H_3PO_4 to remove nonspecific radioactivity. After drying, the paper was subjected to liquid scintillation counting. Data are expressed as means ± S.D.

RESULTS

Insulin Potentiates GABA-induced Cl$^-$ Current and Phosphorylation of the GABA$_A$ Receptor β-Subunit in WT but Not DKO Neurons—In this study, we investigated whether PRIP is involved in insulin-induced GABA$_A$ receptor insertion. We first investigated the effect of insulin on I_{GABA} using acutely isolated hippocampal CA1 neurons from either WT or DKO mice. I_{GABA} was increased maximally by 30% during 15 min of 1 μM insulin stimulation in WT neurons (Fig. 1*A*), which is consistent with previous reports by other groups (10–13). In the DKO neurons, however, no insulin effect was observed (Fig. 1*A*).

We next investigated insulin-induced phosphorylation of the GABA$_A$ receptor β-subunit using cortical neurons from each genotype because insulin-induced membrane insertion of GABA$_A$ receptors is accompanied by the phosphorylation of the β-subunit (11, 12). For this purpose, cultured neurons were metabolically labeled with [^{32}P]orthophosphate for 4 h and then stimulated with 500 nM insulin for 5, 15, or 30 min. The GABA$_A$ receptor β-subunits were precipitated using an anti-GABA$_A$ receptor β2/3-subunit antibody, followed by separation by SDS-PAGE and autoradiography. As shown in Fig. 1*B*, phosphorylation of the GABA$_A$ receptor β-subunit was increased by about 30% after 5 min of insulin stimulation and continued for 30 min in WT, but no such increase in phosphorylation was observed in the DKO neurons. These results suggest that PRIP participates in the insulin-induced phosphorylation of the GABA$_A$ receptor β-subunit, leading to the insulin-induced potentiation of I_{GABA}.

Two possible explanations for the low phosphorylation of the β-subunit observed in DKO neurons are higher activity of phosphatases or lower activity of kinases. We previously reported that PRIP participates in the regulation of the phosphorylation level of the GABA$_A$ receptor β-subunit by acting as a scaffolding protein for protein phosphatases (PP1 and PP2A) (27, 29). So, we investigated the effects of protein phosphatase inhibitors on the insulin-induced potentiation of I_{GABA}. We pretreated neurons with 10 μM okadaic acid for 15 min, which inhibits both PP1 and PP2A at this concentration (42) and then measured the effect of insulin on I_{GABA}. Pretreatment with okadaic acid had no effect on I_{GABA} in the presence of insulin stimulation with DKO neurons (Fig. 2*A*, *right panel*). If higher phosphatase activity is responsible for the low phosphorylation of

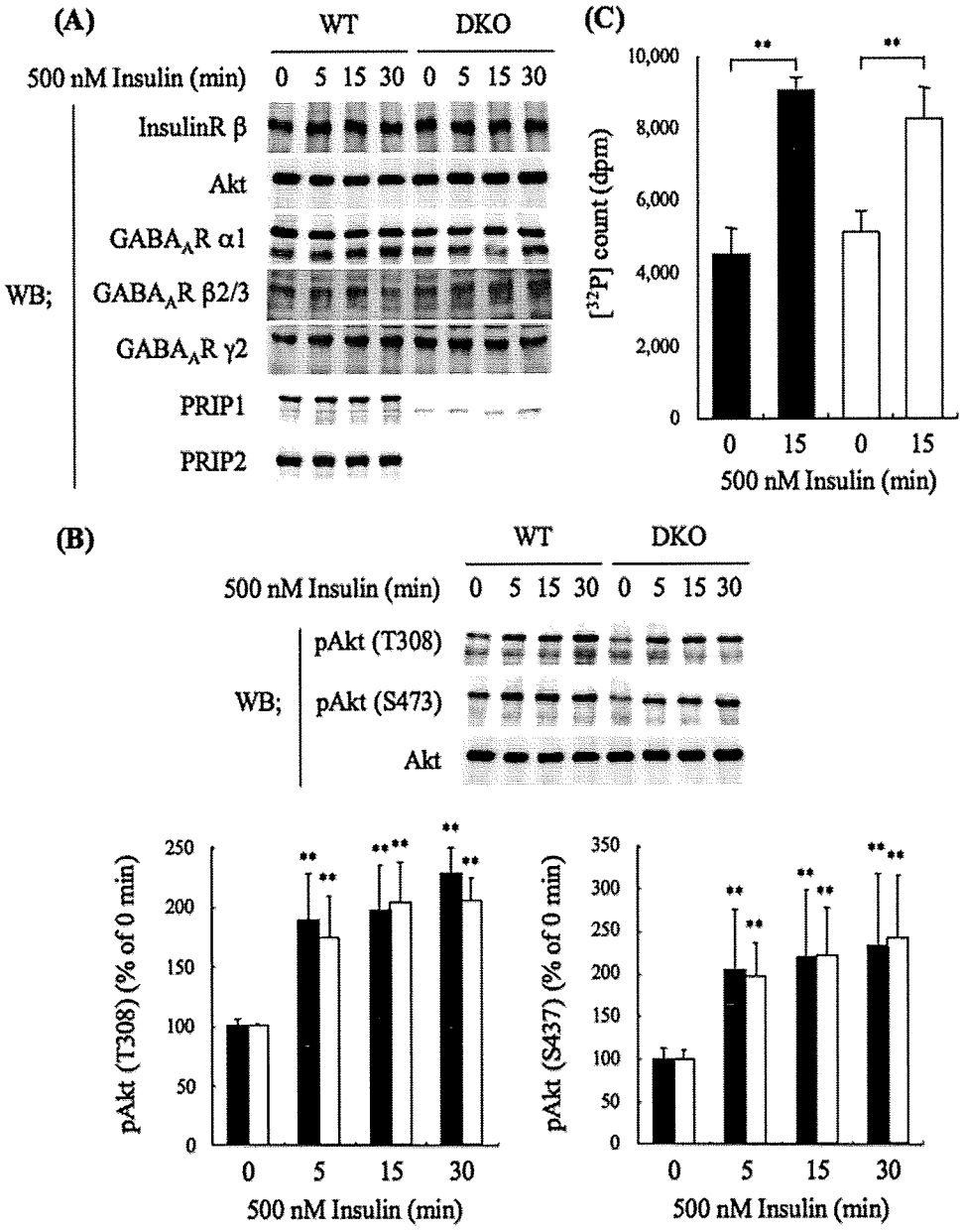

FIGURE 3. **PRIP deficiency caused little changes in the expression level of molecules possibly involved in insulin signaling.** *A*, Western blotting analysis of the expression level of insulin signaling molecules. WT or DKO cortical neurons were cultured for 14–18 days and then stimulated with 500 nM insulin for the indicated time. The cell lysates were analyzed by Western blotting using the indicated antibodies shown on the *left*. The blot shown is a typical result from six experiments. *B*, Western blotting analysis of Akt activation. The WT or DKO cortical cell lysates were prepared in the same way as described above and analyzed by Western blotting using antiphospho-Akt antibodies. The blot and graph shown are a typical result and the summary of seven experiments, respectively. The densities of phospho-Akt at Thr-308 (*left panel*) and Ser-473 (*right panel*) relative to the total amount of Akt are shown. The *filled* and *open columns* represent the results obtained for WT and DKO mice, respectively. *C*, Akt kinase activity assayed *in vitro*. The cell lysates of WT (*filled columns*) or DKO (*open columns*) neurons stimulated with 500 nM insulin for 15 min were subjected to immunoprecipitation using an anti-Akt antibody. The immunocomplexes were subjected to an Akt kinase assay using crosstide as a substrate and [γ-^{32}P]ATP. Data are represented as means ± S.D. (n = 3). Significance was determined by Student's t test (*, $p < 0.05$; **, $p < 0.01$, compared with the result before insulin stimulation), but no difference was detected between WT and DKO.

the β-subunit, okadaic acid would have increased I_{GABA}. WT neurons exhibited a marginal increase of I_{GABA} insulin potentiation, but the effect was not significant (Fig. 2*A*, *left panel*). These results indicate that the PRIP deficiency caused the failure of kinase(s) action, rather than the regulation of phosphatases.

It is well known that insulin activates the phosphatidylinositol 3-kinase (PI 3-kinase)-Akt signaling pathway (43, 44) and the Akt-mediated phosphorylation of the GABA$_A$ receptor β-subunit, and the potentiation of miniature inhibitory postsynaptic currents (mIPSCs) is also reported to require the process (11, 12). We pretreated neurons with 100 nM wortmannin, a potent PI 3-kinase inhibitor (45) for 15 min prior to insulin stimulation. Consistent with previous reports (12, 13), pretreatment with wortmannin completely blocked the insulin potentiation of I_{GABA} in WT neurons (Fig. 2*B*, *left panel*), while wortmannin had no effect on the I_{GABA} in DKO neurons (Fig. 2*B*, *right panel*), confirming that the PI 3-kinase signaling pathway was required in our experiments.

Akt Activation following PI 3-Kinase Activation in Response to Insulin Stimulation—To find reasonable explanations for the failure of the phosphorylation of the GABA$_A$ receptor β-subunit in response to insulin stimulation observed in the DKO neurons, we investigated whether PRIP deficiency impaired the insulin signaling pathway. For this purpose, we first examined the expression level of molecules involved in insulin signaling. Cortical neurons from WT or DKO mice were cultured until 14–18 DIV. After serum starvation for 4 h, the neurons were stimulated with 500 nM insulin for 5, 15, or 30 min, and cell lysates were prepared, followed by Western blotting using relevant antibodies. As shown in Fig. 3*A*, PRIP deficiency had no effect on the expression levels of the insulin receptor β-subunit, Akt, or several GABA$_A$ receptor subunits, and insulin stimulation for up to 30 min also had no effect on the expression of these molecules.

We then examined Akt activation in response to insulin stimulation by monitoring the Akt phosphorylation at the Thr-308 and Ser-473 residues using antiphospho-Akt antibodies. As shown in Fig. 3*B*, the phosphorylation of Akt, an index of Akt activation was increased at 5 min stimulation and sustained for 30 min, which did not differ between the WT and DKO neurons. Wortmannin completely

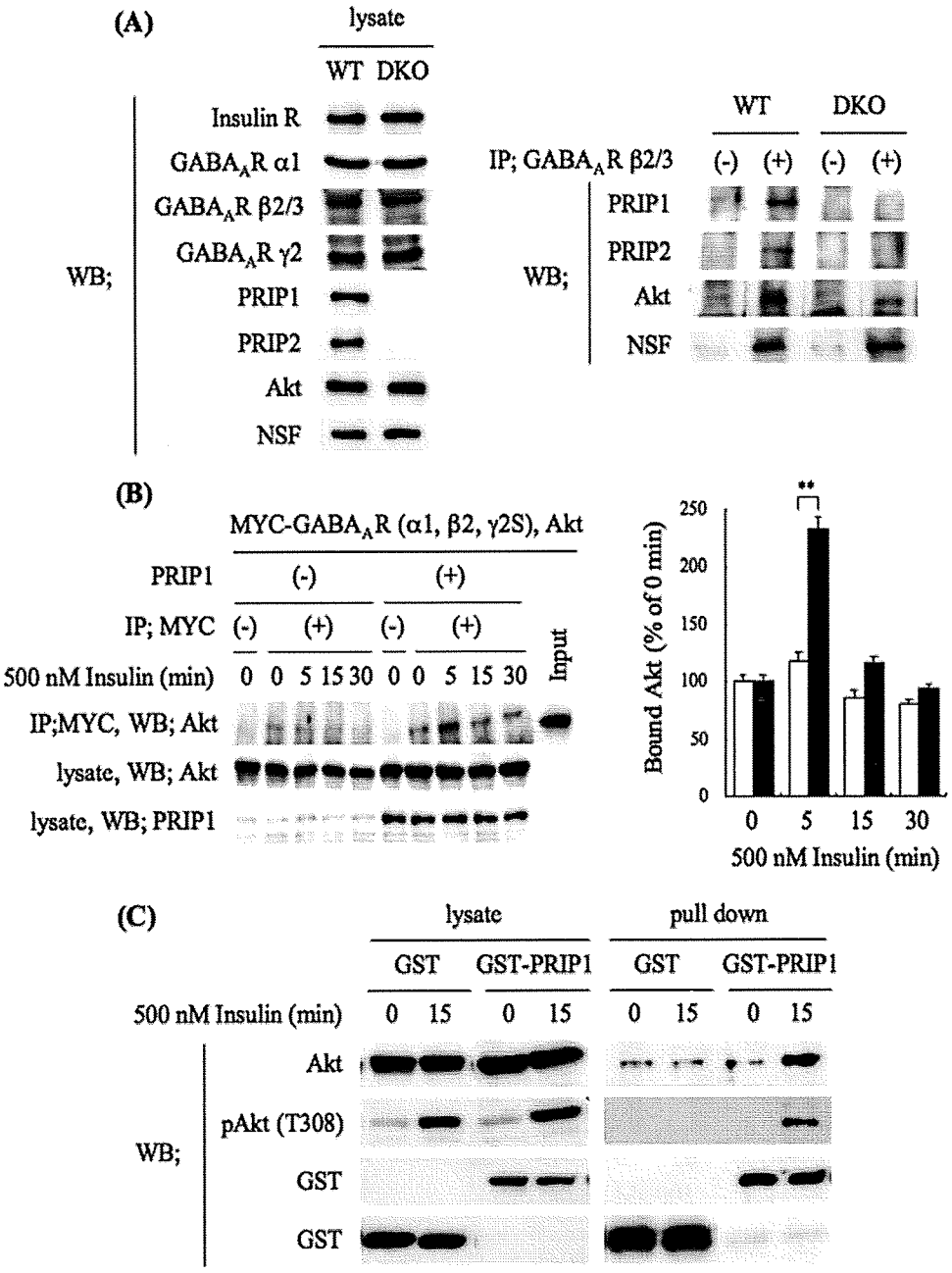

FIGURE 4. **Complex formation among GABA$_A$ receptor, PRIP, and Akt.** *A*, GABA$_A$ receptors were immunoprecipitated using an anti-GABA$_A$ receptor β2/3-subunit antibody from WT or DKO brain lysates. The cell lysates (*left panel*) and immunoprecipitates (*right panel*) were analyzed by Western blotting using the indicated antibodies shown on the *left*. The blots shown are from one of three independent experiments. The other experiments gave similar results. *B*, Myc-tagged GABA$_A$ receptor subunits (α1, β2, and γ2S) and Akt with or without PRIP1 were exogenously expressed in HEK293 cells. After stimulation with 500 nM insulin for the indicated time, the cell lysates were subjected to immunoprecipitation using an anti-Myc antibody. The immunocomplexes were separated by SDS-PAGE and then analyzed by Western blotting using an anti-Akt antibody. The cell lysates were also analyzed by Western blotting using the indicated antibodies. The blots shown are one of three independent experiments. The other experiments gave similar results. The graph shows quantitative data concerning the Akt co-precipitated with GABA$_A$ receptors in PRIP expressing (*filled columns*) or control (*open columns*) cells. Significance was determined using the Student's *t* test (**, $p < 0.01$ from the control cells without exogenous PRIP1). *C*, HEK293 cells were transfected with Akt and GST-PRIP1 (or GST) expression plasmids. After stimulation with 500 nM insulin for 15 min, GST fusion proteins were precipitated with glutathione-Sepharose™ 4B. The protein complexes were separated by SDS-PAGE and then analyzed by Western blotting using an anti-Akt antibody, an antiphospho-Akt (Thr-308), and an anti-GST polyclonal antibody. The cell lysates were also analyzed by Western blotting using the indicated antibodies. The blots shown are one of three independent experiments. The other experiments gave similar results.

blocked the increase in phospho-Akt (results not shown). The activity of Akt was biochemically assayed: immunoprecipitates of anti-Akt antibody attached to WT or DKO neurons stimulated with insulin for 15 min were subjected to an Akt kinase assay *in vitro* using crosstide as a substrate and [γ-^{32}P]ATP. As shown in Fig. 3*C*, the immunoprecipitates from the neurons stimulated with insulin exhibited an ~2-fold increase of ^{32}P radioactivity incorporation, and there was no significant difference between the genotypes. The results indicate that Akt kinase activation, which is probably responsible for insulin-induced phosphorylation of the GABA$_A$ receptor β-subunit (11, 12), was not impaired by PRIP deficiency.

PRIP Facilitates Complex Formation between GABA$_A$ Receptors and Akt—Because PRIP deficiency had no effect on insulin-induced Akt activation but caused the impairment of the insulin-induced phosphorylation of the GABA$_A$ receptor β-subunit, we hypothesized that PRIP might function as a scaffolding molecule that makes Akt more accessible to the GABA$_A$ receptor β-subunit. To examine this possibility, we performed a co-immunoprecipitation assay using brain lysates. The brain lysates prepared from WT or DKO mice were immunoprecipitated using an anti-GABA$_A$ receptor β2/3-subunit and then analyzed by Western blotting using anti-PRIP1, anti-PRIP2, and anti-Akt antibodies. Assessment by Western blotting of the amount of immunoprecipitated GABA$_A$ receptor β2/3-subunits was not possible because the corresponding bands overlapped with that for the immunoglobulin heavy chain used for the immunoprecipitation. However, we confirmed in advance that the antibody we used was able to precipitate the GABA$_A$ receptor β-subunit using a HEK293 reconstitution system with GABA$_A$ receptor subunits in combination with the [^{35}S]methionine pulse-chase technique (results not shown). Consistent with our previous reports (27, 28), PRIP1 and -2 in the WT brain lysates were co-immunoprecipitated with the GABA$_A$ receptor β-subunit (Fig. 4*A*, *right panel*). There were no corresponding bands for PRIP1 or 2 in the immunocomplexes produced from the DKO brain lysates (Fig.

4*A*, *right panel*). The amount of Akt co-precipitated with the GABA$_A$ receptor β2/3-subunit was much greater in the WT lysates than in the DKO lysates (Fig. 4*A*, *right panel*), indicating that PRIP promotes complex formation between the β2/3-subunit and Akt. It is noteworthy that PRIP deficiency caused no effect on the direct binding between GABA$_A$ receptor β2/3-subunit and NSF, one of the β-subunit-binding proteins (46) (Fig. 4*A*, *right panel*). We next investigated whether insulin affects this complex formation, using a cultured reconstitution system. We exogenously expressed Myc-tagged GABA$_A$ receptor subunits (α1, β2, and γ2S) and Akt, with or without PRIP1 in HEK293 cells, which intrinsically contain trace amounts of PRIP1 and 2. After insulin stimulation for 5, 15, or 30 min, the cell lysates were subjected to immunoprecipitation using an anti-Myc antibody, followed by Western blotting for Akt. The amount of immunoprecipitated GABA$_A$ receptors was not apparent for the same reason as mentioned above. A small amount of Akt was seen in fractions co-precipitated with GABA$_A$ receptors in the nonstimulated cells. Insulin stimulation only increased the amount of Akt co-precipitated with GABA$_A$ receptors in the PRIP-expressing cells (Fig. 4*B*, the left and right panels show typical blots and a summary of multiple experiments, respectively), suggesting that PRIP facilitates complex formation between the GABA$_A$ receptor and Akt under insulin stimulation.

We next examined the direct binding between PRIP1 and Akt using an *in vivo* GST pull-down assay. Genes for GST or GST-rat(r)PRIP1 were transfected with Akt into HEK293 cells. After insulin stimulation for 15 min, GST alone or GST-rPRIP1 was precipitated from the cell lysates using glutathione-conjugated beads, followed by Western blotting for Akt and phospho-Akt. As shown in Fig. 4*C*, GST-rPRIP1, but not GST, bound to Akt when the cells were stimulated with insulin. Taken together, these results suggest that PRIP recruits phosphorylated (active) Akt to GABA$_A$ receptors by forming a ternary complex under insulin stimulation. Thus, PRIP might be implicated in Akt-dependent phosphorylation of GABA$_A$ receptors, leading to their insertion into the cell surface membrane.

PRIP1-(553–565) Peptide Attenuates Insulin Potentiation of I_{GABA}—We next investigated whether such complex formation is important for the insulin potentiation of I_{GABA}. To address this issue, PRIP1-(553–565) peptide at 3 μg/ml, which reduces the binding between PRIP1 and GABA$_A$ receptor β-subunit in cultured cells (29), was applied into WT neurons through a patch pipette, and then I_{GABA} was measured in the presence of insulin. As shown in Fig. 5, the PRIP1-(553–565) peptide but not the control peptide (scrambled peptide of PRIP1-(553–565)) partially attenuated the insulin potentiation of I_{GABA}, indicating that the association between the β-subunit and PRIP is important for making Akt accessible to the receptor β-subunit, resulting in the potentiation of I_{GABA}.

BFA Reverses the Effect of Insulin on I_{GABA}—Insulin triggers the activation of Akt, leading to the phosphorylation of GABA$_A$ receptors, which are resistant to internalization, by inhibiting its association with AP2 complex (6–9). Therefore, the apparent potentiation of I_{GABA} observed in WT neurons could have resulted from the inhibition of insulin-induced internalization

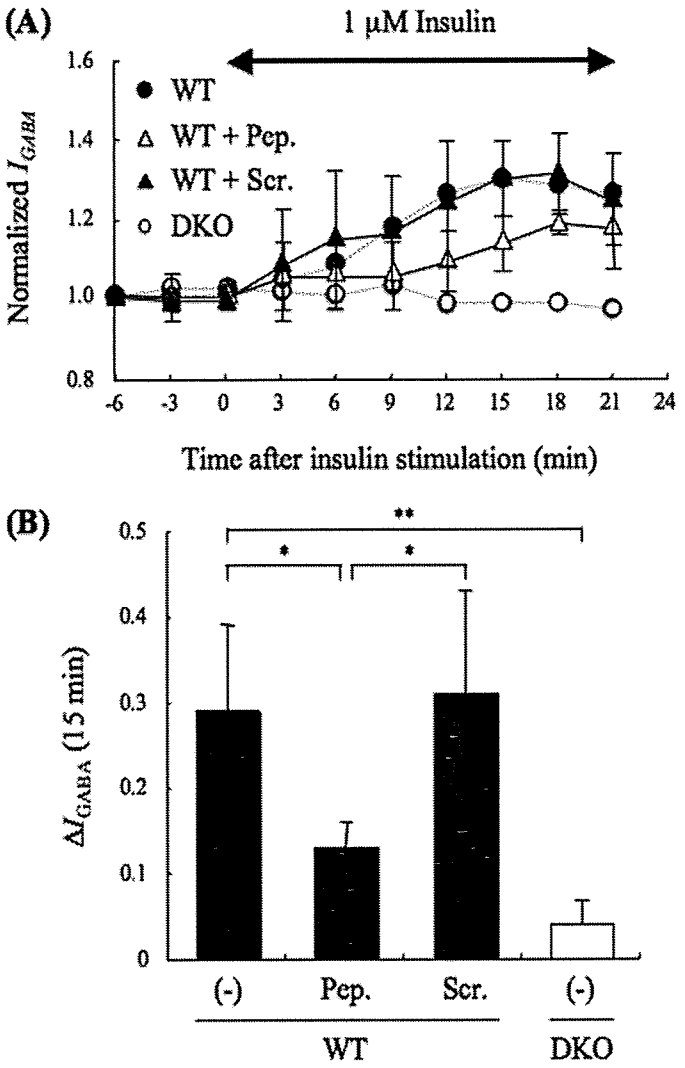

FIGURE 5. **Effect of PRIP1-(553–565) peptide on insulin potentiation of I_{GABA} in hippocampal CA1 neurons.** *A*, PRIP1-(553–565) peptide (3 μg/ml) (*open triangles*, $n = 3$), which diminishes the binding between PRIP and the GABA$_A$ receptor β-subunit (29), or its scramble peptide (3 μg/ml) (*closed triangles*, $n = 3$) were introduced using a patch pipette. The experiment was performed in the same way as that shown in Fig. 1*A*. A *double-headed arrow* indicates the time period of insulin application. Data are represented by the means ± S.D.. The I_{GABA} from WT (*closed circles, dashed line*) or DKO (*open circles, dashed line*) mice without the peptide, which were taken from those shown in Fig. 1*A*, are also shown as references. *B*, graph shows the potentiation of I_{GABA} at 15 min after insulin stimulation in WT (*filled columns*) or DKO (*open column*) neurons with or without the indicated peptides (*Pep.*, PRIP1-(553–565 peptides); *Scr.*, PRIP1-(553–565) scramble peptides; (−), no peptides). Data are represented as means ± S.D. Significance was determined using the Student's *t* test (*, $p < 0.05$; **, $p < 0.01$, between indicated two columns).

rather than insulin-induced facilitation of GABA$_A$ receptor insertion. To examine this possibility, we pretreated WT neurons with 5 μg/ml BFA, an inhibitor of anterograde trafficking from the ER to the Golgi (32, 33) for 15 min and measured the effect of insulin on I_{GABA}. If the assumption is correct, BFA would have had little effect; however, BFA caused further decreases in I_{GABA} below the control level after insulin treatment (Fig. 6, *left panel*). This effect was not observed under nonstimulated conditions (time: −6 to 0 min) (Fig. 6, *left panel*). BFA had no effect on I_{GABA} in the DKO neurons (Fig. 6, *right panel*). The results suggest that insulin induces both

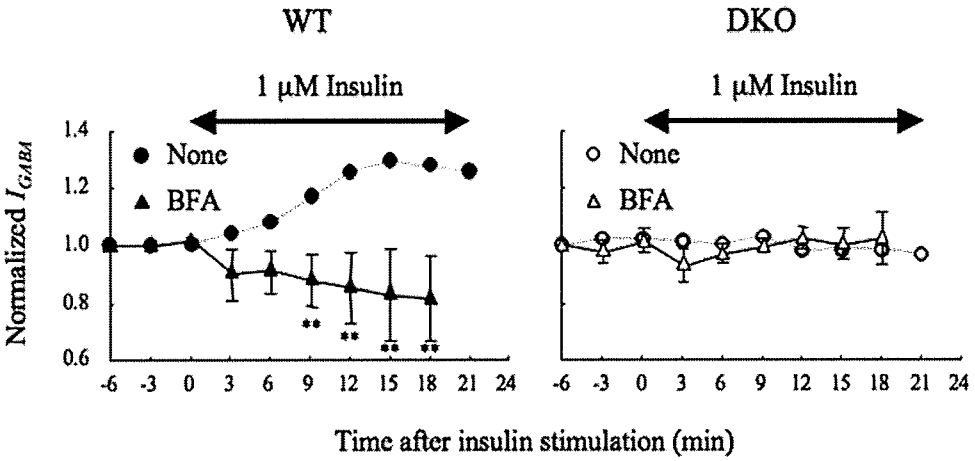

FIGURE 6. **Effect of BFA on insulin potentiation of I_{GABA}.** Neurons from either WT (*left panel, closed triangles, n* = 3) or DKO (*right panel, open triangles, n* = 3) were pretreated with 5 μg/ml of BFA, which inhibits anterograde trafficking from the ER to the Golgi apparatus (32, 33) for 15 min and throughout the experiment. The experiment was performed in the same way as that described for Fig. 1*A*. All data are represented as means ± S.D. The I_{GABA} from either WT or DKO without BFA, which were taken from those shown in Fig. 1*A*, are also shown as references. Significance was determined using the Student's *t* test (**, $p < 0.01$, from the results obtained in the absence of the drug). *Double-headed arrows* indicate the time period of insulin stimulation. *none*, no drug; *BFA*, brefeldin A.

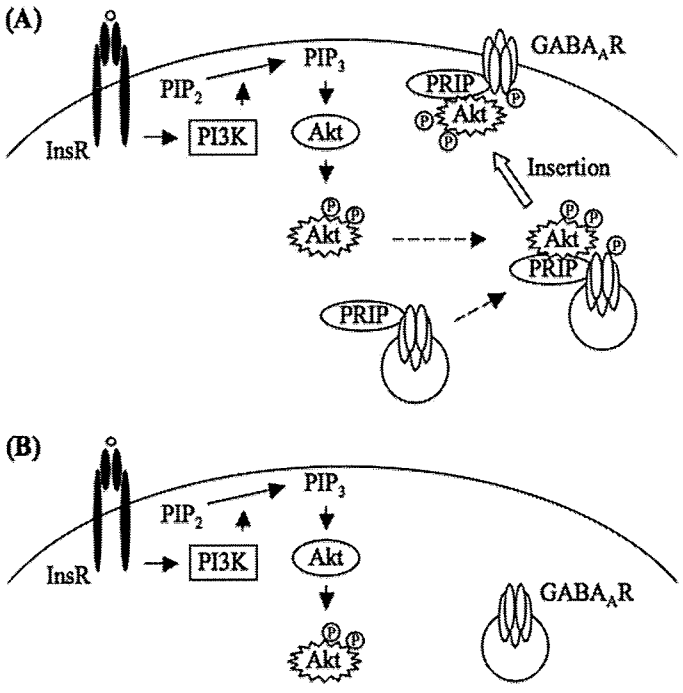

FIGURE 7. **Schematic representation of the role of PRIP in insulin-induced membrane insertion of GABA$_A$ receptors.** *A*, insulin stimulation induces Akt activation in a PI 3-kinase-dependent manner. Subsequent phosphorylation of the β-subunits of GABA$_A$ receptors by Akt is facilitated by PRIP through the ternary complex formation with activated Akt and β-subunit, which triggers an enhancement of the insertion of GABA$_A$ receptors into the postsynaptic membrane. *B*, absence of PRIP fails in making activated Akt accessible to β-subunit. *Arrows* indicate the signaling pathways to activate downstream target. *Dashed arrows* indicate the complex formation. *White arrow* indicates membrane insertion of GABA$_A$ receptor. *InsR*, insulin receptor; *GABA$_A$R*, GABA$_A$ receptor, *PI3K*, PI 3-kinase; *PIP$_2$*, phosphatidylinositol 4,5-bisphosphate; *PIP$_3$*, phosphatidylinositol 3,4,5-trisphosphate, *PRIP*, PLC-related but catalytically inactive protein. *Circled P* indicates the phosphorylation.

GABA$_A$ receptor insertion and subsequent endocytosis of the GABA$_A$ receptor and that this insertion mainly occurs in WT neurons. Additionally, the result indicates that PRIP is an important molecule in the mechanism that allows insulin to execute its effects on GABA$_A$ receptor trafficking.

DISCUSSION

It has been reported that insulin triggers rapid translocation of functional GABA$_A$ receptors from the intracellular pool to the cell surface membrane, thus increasing the amplitude of GABA$_A$ receptor-mediated mIPSCs (10). The underlying molecular mechanisms have been proposed as follows: insulin elicits tyrosine phosphorylation at residues Tyr-372 and Tyr-379 of the β2-subunit of GABA$_A$ receptors by unknown kinase(s), and these phosphotyrosines are then recognized by the SH2 domain of p85 (13), a regulatory subunit of PI 3-kinase. The PI 3-kinase bound to GABA$_A$ receptors produces phosphatidylinositol 3,4,5-trisphosphate, an upstream activator of serine/threonine kinase Akt around the receptors, leading to the phosphorylation of the intracellular loop region of the β-subunits (Ser-409 in β1, Ser-410 in β2, or Ser-409 in β3), which is essential for the membrane insertion of GABA$_A$ receptors (11, 12).

The current study was motivated by the finding that no effect of insulin on the potentiation of I_{GABA} was seen in neurons derived from PRIP-deficient mice, indicating that PRIP is involved in process(es) triggered by insulin stimulation. Therefore, our studies exploring the possible mechanisms in which PRIP is implicated have continued to examine each step involved in known insulin signaling pathways (43, 44). PRIP deficiency neither perturbs protein expression profiles including those of insulin receptors and Akt nor impairs the activation of Akt in whole cell extract, as assessed by the phosphorylation of residues Thr-308 and Ser-473 and *in vitro* enzymatic activity using synthetic peptide substrate. However, the phosphorylation of the GABA$_A$ receptor β-subunit in neurons from DKO mice was not augmented by insulin stimulation. This phenomenon is probably attributed to the fact that Akt is not accessible to GABA$_A$ receptor β-subunits in the absence of PRIP. Based on the observations, we propose that PRIP functions as a scaffolding protein that presents the active form of Akt to GABA$_A$ receptors, enabling insulin signaling to potentiate I_{GABA} (Fig. 7).

We previously reported that PRIP is involved in the regulation of BDNF-induced endocytosis of GABA$_A$ receptors (29). In this case, PKC, which directly associates with the GABA$_A$ receptor β-subunit, is activated by BDNF stimulation and triggers the phosphorylation of the Ser-408 and Ser-409 residues of the β3-subunit. These residues are subsequently dephosphorylated by PP2A, which is recruited to the vicinity of the receptors via PRIP (29, 41). Thus, BDNF stimulation triggers transient phosphorylation of the β-subunit, followed by long-lasting dephosphorylation. The μ2-subunit of AP2 complex